


RESEARCH ARTICLE

Open Access



Geophysical investigation of the Mado Megamullion oceanic core complex: implications for the end of back-arc spreading

Kyoko Okino^{1*} , Kenichiro Tani², Masakazu Fujii^{3,4}, Fei Zhou⁵, Osamu Ishizuka⁶, Yasuhiko Ohara^{7,8,9}, Tomoko Hanyu¹⁰ and Yuki Matamura¹¹

Abstract

Detachment faulting is one of the main styles of seafloor spreading at slow to intermediate mid-ocean ridges. However, we have limited insight into its role in back-arc basin formation. We surveyed a remnant back-arc spreading center in the Philippine Sea and determined the detailed features and formation processes of the Mado Megamullion (Mado MM) oceanic core complex (OCC). This was undertaken in the context of back-arc evolution, based on the ship-borne bathymetry, magnetics, and gravity with radiometric age dating of the rock samples collected. The Mado MM OCC has a typical OCC morphology with prominent corrugations on the domed surface and positive gravity anomalies, suggesting that there has been an exposure of the lower crust and mantle materials by a detachment fault. The downdip side of the detachment continues to the relict axial rift valley, which has indicated that the Mado MM OCC was formed at the end of the back-arc basin opening. The spreading rate of the basin decreased once when the spreading direction changed after six million years of stable trench perpendicular spreading. The rate then further decreased immediately prior to the end of the spreading when the Mado MM OCC was formed. The existence of other OCC-like structures in the neighboring segment and the previously reported OCCs along the Parece Vela Rift have indicated that the melt-poor, tectonic-dominant spreading is a widespread phenomenon at the terminal phase of back-arc spreading. The decrease in spreading rate in the later stage is consistent with the previous numerical modeling because of the decrease in trench retreat. In the Izu–Bonin–Mariana arc trench system, the rotation of the spreading axis and the resultant axis segmentation have enhanced the lithosphere cooling and constrained mantle upwelling, which caused the tectonic-dominant spreading at the final phase of the basin evolution.

Keywords Geophysical mapping, Rock age dating, Back-arc basin, Oceanic core complex, Detachment, Mid-ocean ridge process, Oceanic crust

*Correspondence:

Kyoko Okino

okino@aori.u-tokyo.ac.jp

Full list of author information is available at the end of the article



© The Author(s) 2023. **Open Access** This article is licensed under a Creative Commons Attribution 4.0 International License, which permits use, sharing, adaptation, distribution and reproduction in any medium or format, as long as you give appropriate credit to the original author(s) and the source, provide a link to the Creative Commons licence, and indicate if changes were made. The images or other third party material in this article are included in the article's Creative Commons licence, unless indicated otherwise in a credit line to the material. If material is not included in the article's Creative Commons licence and your intended use is not permitted by statutory regulation or exceeds the permitted use, you will need to obtain permission directly from the copyright holder. To view a copy of this licence, visit <http://creativecommons.org/licenses/by/4.0/>.

1 Introduction

Detachment faulting is now recognized as an important style of seafloor spreading in global mid-ocean ridge systems. Oceanic core complexes (OCCs) exposed along long-lived detachments and associated asymmetric spreading have been reported in ultraslow (e.g., Searle et al. 2003; Cannat et al. 2006; Hayman et al. 2011; Sauter et al. 2013; Grevemeyer et al. 2018; Haughton et al. 2019; Corbalán et al. 2021), slow (Cann et al. 1997, 2015; Tucholke et al. 1998, 2008; Ranero and Reston 1999; Smith et al. 2006, 2014; Escartín et al. 2008), and intermediate spreading ridges (Okino et al. 2004). However, to date, there have been relatively few studies on OCCs in back-arc spreading centers, despite back-arc systems being an indispensable part of global divergent boundaries and the OCCs being a tectonic window to the mantle beneath back-arc areas.

The most extensively studied OCC in a back-arc setting is the Godzilla Megamullion (GMM) OCC in the Parece Vela Basin in the Philippine Sea (e.g., Ohara et al. 2001; Harigane et al. 2008, 2011a, b; Tani et al. 2011; Loocke et al. 2013; Spencer and Ohara 2014; Ohara 2016). This OCC extends 125 km in spreading direction and is located adjacent to the extinct spreading axis, which is known as the Parece Vela Rift (Okino et al. 1998). Zircon dating of gabbroic samples collected has indicated that the GMM was formed between approximately 13–8 Ma (Tani et al. 2011). This result suggests that tectonic spreading with low melt supply was dominant in the last five million years in this back-arc basin formation. If OCCs and/or other structures have suggested that detachment faulting spreading is widely distributed along extinct spreading axes in the Philippine Sea, this likely indicates that the reduction of melt supply is a common feature in the final stage of back-arc basin formation and that the back-arc system crosses a threshold in melt supply, triggering detachment faulting. Then, the extensional stress field likely continues for millions of years after magma production has waned.

The origin of back-arc basins has been extensively debated in the literature. There are two major models, that is, trench roll-back (Elsasser 1971; Molnar and Atwater 1978; Hall et al. 2003; Schellart 2005) and slab-anchor (Chase 1978; Scholz and Campos 1995). Cyclic back-arc spreading that has been observed at the Mariana arc and the Tonga arc has indicated the occurrence of a non-steady-state process controlled by some common physical/chemical conditions in back-arc areas. Some numerical model studies (Nakakuki and Mura 2013; Schellart and Moresi 2013; Ishii and Wallis 2022) have proposed potential control factors. However, we have not yet entirely determined the mechanisms governing the back-arc extension and formation of basins. Sdrolias and

Müller (2006) compiled the past and current absolute plate motions and concluded that the absolute motion of the overriding plate preceded the back-arc opening and that trench roll-back was dominant after the opening started. The spreading process and magma generation were significantly influenced by arc magmatism in the early stage of spreading but were similar to those of mid-ocean ridges in mature back-arc basins (Arai and Dunn 2014). Important questions remain around how and why back-arc basins ceased to be opening after 10 million years of spreading. To address these questions, we need to examine inactive back-arc basins where the spreading has already stopped.

The Mado MM OCC is an OCC at the southern end of the Shikoku Basin in the Philippine Sea. It is located adjacent to the extinct spreading axis, and its size and morphologies are similar to typical OCC that have previously been reported in mid-ocean ridges such as the Kane Megamullion (Dick et al. 2008; Lissenberg et al. 2016; Xu and Tivey 2016; Harigane et al. 2016; Xu et al. 2020), Atlantis Massif (Nooner et al. 2003; Schroeder and John 2004; Karson et al. 2006; Grimes et al. 2008; Collins et al. 2009, 2012), and the 13° 20' OCC (Smith et al. 2006; Craig and Parnell-Turner 2017; Escartín et al. 2017; Parnell-Turner et al. 2017; Searle et al. 2019). We conducted a series of research cruises at the Mado MM OCC and adjacent areas from 2018 to 2021 and collected geophysical data and rock samples (Basch et al. 2020; Akizawa et al. 2021; Hirauchi et al. 2021; Sen et al. 2021). This paper presents an overview of the geophysical features of the area and the rock age dating from our recent surveys. We describe the details of the morphological and geophysical features of the Mado MM OCC and the surrounding area as well as determining its structure and formation processes. We discuss the relationship between the Mado MM OCC formation and the history of the Shikoku Basin and suggest the occurrence of tectonic-dominant spreading at the final stage of back-arc spreading in general, in reference to other OCCs that have been reported near the extinct back-arc spreading centers.

2 Regional setting

The Philippine Sea comprises active and inactive island arcs, back-arc basins, and fragments of continental crust (Fig. 1). The Pacific Plate subducts beneath the Philippine Sea Plate, causing back-arc rifting of the Izu–Bonin arc (Taylor 1992; Ishizuka et al. 1998; Hochstaedter et al. 2000; Takahashi et al. 2009) and back-arc spreading behind the Mariana arc (Fryer 1996; Yamazaki and Murakami 1998; Deschamps and Fujiwara 2003; Kitada et al. 2006; Fujiwara et al. 2008; Takahashi et al. 2008). West of these present-day active back-arc zones, the Shikoku and the Parece Vela Basins were formed in

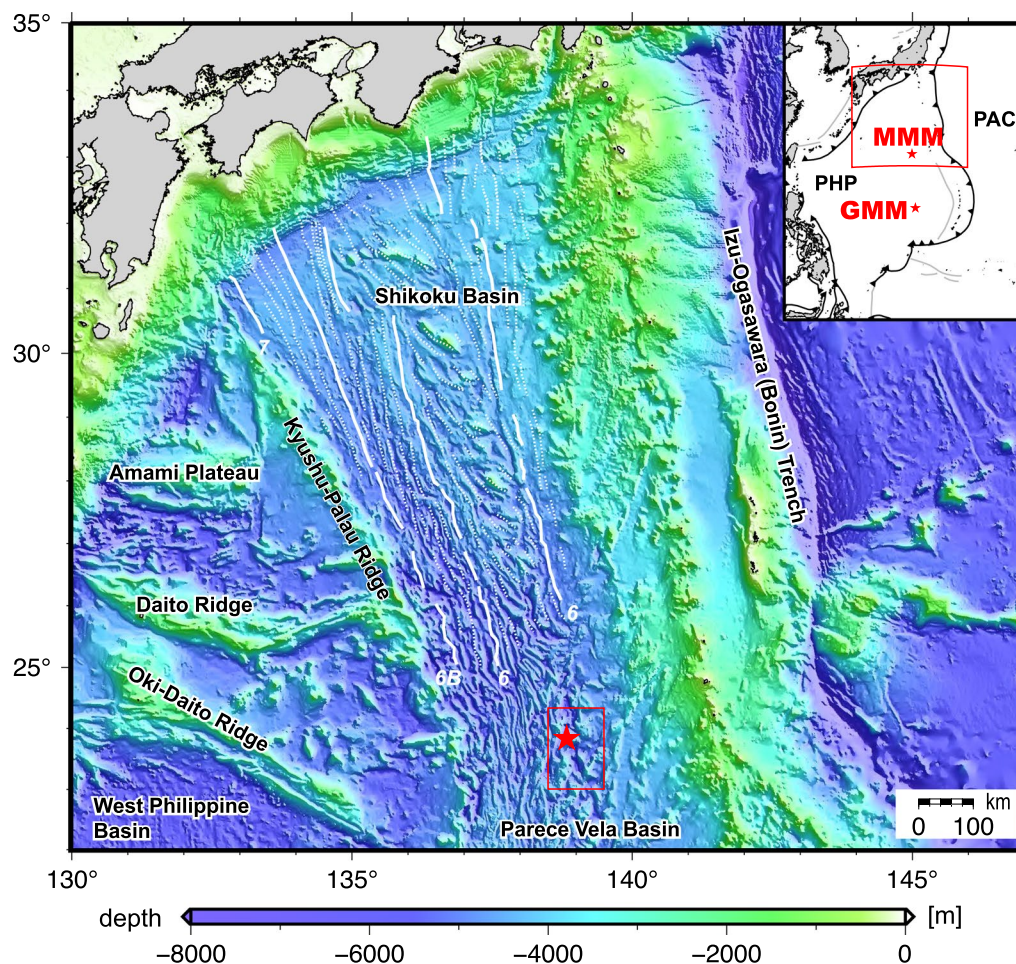


Fig. 1 Geological and tectonic setting of the Shikoku Basin and the adjacent area. Major magnetic isochrons are shown (Okino 2015). The box shows the survey area of this study. The loci of the Mado Megamullion (MMM) OCC and the Godzilla Megamullion (GMM) are shown

mid-Oligocene to Miocene time, rifting the paleo Izu–Bonin–Mariana arc crust (e.g., Okino et al. 1999; Lallemant 2016).

The Shikoku Basin is one of the most intensively studied back-arc basins worldwide, and its evolution process has been determined predominantly based on its prominent lineated magnetic anomaly pattern (Fig. 1; Tomoda et al. 1975; Okino et al. 1994; Sdrolias et al. 2004; Okino 2015), and the radiometric age dating along the remnant Kyushu–Palau Ridge (Ishizuka et al. 2011), and the seamounts located near the remnant spreading center known as the Kinan Seamount Chain (Sato et al. 2002; Ishizuka et al. 2009). These previous studies have suggested the following basin history. The proto-Izu–Ogasawara arc was rifted at approximately 26 Ma, and the earlier east–west spreading was followed by NE–SW spreading at a later stage. The basin ceased to open around 15 Ma, with some alkalic volcanism continuing sporadically after the basin formation, forming the Kinan

Seamount Chain. The Parece Vela Basin, which is located south of 25° N, has a similar history to the paleo Mariana arc (Mrozowski and Hayes 1979; Okino et al. 1998; Ishizuka et al. 2004; Sdrolias et al. 2004; Okino 2015). Detailed reconstructions of the spreading history are still being debated mainly because of weak magnetic anomalies and the significant presence of unsurveyed areas in its southern section. However, the two basins were linked at approximately 19 Ma and evolved since then as one system (Okino 2015).

The Mado MM OCC was first fully mapped in 2018 and is located at 23° 40' N, at the junction of two basins (Fig. 1, red box). The axial zone of the Shikoku Basin is characterized by the Kinan Seamount Chain, the overprint of post-spreading alkalic volcanism to the north of 26° 30' N (Ishii et al. 2000; Sato et al. 2002; Ishizuka et al. 2009), whereas the axial rift structure is located to the south. The Mado MM OCC has developed at the remnant inside corner of the axial rift, where the spreading

among all the lines and applied the dc-shift smaller than 11 nT to minimize the cross-over errors. We produced a 1500 m-interval grid of the magnetic anomalies which was then reduced to pole to remove the skewness. Here, we assumed the inclination of the magnetized body as being 33°, considering the geocentric axial dipole field at the paleo latitude being 18°N, for approximately 5° northward shift of the Philippine Sea Plate since middle to late Oligocene which was estimated from paleomagnetic analysis of the drilled core (Yamazaki et al. 2021). We also calculated the equivalent magnetization of the area assuming a uniformly magnetized 0.5 km-thick layer draping seafloor morphology, following the methods of Parker and Huestis (1974) and Macdonald et al. (1980). To identify the geochrons and magnetic structure over the OCC, we conducted a two-step forward modeling. We first constructed a standard one-layer block model to obtain a general idea of the spreading history and then produced a three-layer model with different remnant magnetization values developed as Zhou and Dymant (2022) and Zhou et al. (2022) for more detailed discussion. Both forward models assumed that the magnetic anomalies recorded the spreading history sequentially. This assumption is appropriate for the volcanic seafloor with well-ordered abyssal hills, but not generally correct for OCCs, where the detachment fault zone influences the magnetic signals. The examination of this issue is shown in Discussion section.

We also collected data on the vector magnetic field using shipboard fluxgate magnetometer system. The permanent and induced ship magnetizations were removed, using figure eight maneuvers conducted at different latitudes in each cruise (Isezaki 1986). The absolute values were less reliable. However, the variation of each component of the magnetic field has been well recorded. We calculated the ISDV (Intensity of Spatial Differential Vectors) (Seama et al. 1993) and determined the location and direction of the magnetic boundaries. We used the revised STCM (Shipboard Three-Component Magnetometer) kit originally provided by Korenaga (1995) to process and calculate the vector anomaly data.

The shipboard gravity data were obtained during KH-18-2 and YK18-07 using ZLS D-004 (R/V *Hakuho-maru*) and Lacoste-Romberg S-63 (R/V *Yokosuka*), respectively. The absolute gravity tie was conducted at Yokosuka port, Japan. We calculated the free-air gravity anomaly, subtracted the International Gravity Formula 1980, and Eötvös correction was applied. We also used the existing gravity anomaly data in the NGDC Marine Trackline Geophysics Database, in line with the total magnetic anomaly, and merged the data with our newly collected data. The dc-shift smaller than 4.5 mGal was applied to minimize the cross-over errors and to fit the

satellite altimetry data. We developed a 1500 m-grid of free-air anomaly and then calculated the mantle Bouguer anomaly (MBA) assuming 1665 and 600 kg/m³ density contrast at the seafloor and Moho, respectively. We did not calculate the residual mantle Bouguer anomaly (RMBA), because (1) the reliable age estimation for the entire area is challenging at present, and (2) the area is a relict spreading center of at least older than 13 Ma in age and the variation in the cooling effect is relatively low at less than 5 mGal. We estimated the crustal thickness variation using MBA, assuming that the density contrast was uniform and that all the MBA occurred because of the crustal thickness variation (Kuo and Forsyth 1988). We also estimated the density variation, assuming a uniform crustal thickness of 6 km.

4 Results

4.1 Morphology

Figure 2 shows the shaded bathymetry (Fig. 2a) and the interpreted morphological features of the Mado MM OCC and the adjacent areas (Fig. 2b). The Shikoku/Parece Vela back-arc basin floor becomes narrowest between the remnant and present arcs in this area (Fig. 1), where the early east–west spreading stage started at approximately 22 Ma (Okino 2015). We can recognize nearly N–S trending abyssal hills at the westernmost edge of the survey area. In contrast, the eastern counterpart is unclear due to the thick sediment cover supplied by eastern arc volcanism. The central part is dominated by NW–SE trending abyssal hills, suggesting NE–SW spreading in the later stage of basin formation. The rift axis trends N128° E and is right-laterally offset by prominent NE–SW fracture zones.

There are at least three pronounced detachment-related structures in the area. The Mado MM OCC is located at the northeastern side of the relict axial rift and is a domed massif with flow-line parallel corrugations (Fig. 2b). It is adjacent to the remnant transform fault that offsets the spreading axis 51 km. The length of the rift segment, hereafter referred to as the Mado segment, is 46 km, and half is the width of the domed part of the Mado MM OCC. East of the Mado segment, we can also recognize a clear corrugated surface on the northeastern side of the relict axis. The corrugation extends more than 40 km, whereas the width of the corrugated surface is less than 18 km. We have tentatively called this structure 23° 20' N OCC. This OCC is also adjacent to the remnant transform fault, which offsets the remnant ridge axis 34 km. At the intersection of the Mado segment axis and the remnant transform fault, a semicircular domed high with an 18 km diameter has developed. We did not identify any clear corrugations here, but the morphological feature and the location have indicated that this high

is what is known as a non-transform offset (NTO) massif (Gràcia et al. 2000).

The bathymetry of Mado MM has the typical OCC morphology (Fig. 3), considered as the exhumation of the lower crust and mantle rocks by a detachment fault. The length and width of the Mado MM OCC are 23 and 25 km, respectively, and this size is as same as the well-surveyed Kane Megamullion (Dick et al. 2008; Lissenberg et al. 2016; Xu and Tivey 2016; Harigane et al. 2016; Xu et al. 2020) and the Atlantis Massif (Nooner et al. 2003; Schroeder and John 2004; Karson et al. 2006; Grimes et al. 2008; Collins et al. 2009, 2012) along the Mid-Atlantic Ridge. The relatively large-scale corrugation with a 5.5 km wavelength is dominant on the entire surface, and substantially smaller-scale striations are also identified (Fig. 3b). The wavelength of the smaller-scale striations is ~100 m order, for our observations were limited by ~50 m resolution of ship-mounted multibeam sonar. These striations can be seen over the large-scale corrugations, and each striation extends a few kilometers at most in the flow-line direction. The breakaway is ~30 km from the relict axial rift (Fig. 3b). The termination, i.e., the hanging wall cutoff of the detachment fault, continues

to the axial rift valley, which suggests that the detachment faulting occurred at the end of the back-arc basin opening. The width of the OCC is wider at the breakaway and narrowed toward the termination. This change is explained by along-axis gradients in the melt supply rate (Howell et al. 2019). A horseshoe-shaped depression on the slope near the termination is likely a signature of mass wasting after the denudation of the OCC (Fig. 3a and c). Slope debris is distributed at the bottom of the slope. Mass wasting near OCC terminations has often been observed in other OCCs (Cannat et al. 2013; Escartín et al. 2017, 2022). Although flow-line parallel corrugations and striations dominate at the surface, several rift-parallel lineaments have also been observed, which are likely post-detachment extensional structures.

The opposite side of the Mado MM OCC is characterized by a well-ordered abyssal hills pattern (Fig. 2b). The direction of the abyssal hill continuously changes from N178° E at 138° 20' E to N128° E close to the relict axial rift. The fracture zone is perpendicular to the abyssal hill, and the general geometry shows an S-shaped curve as a consequence. These observations have suggested that there has been a gradual change in the spreading

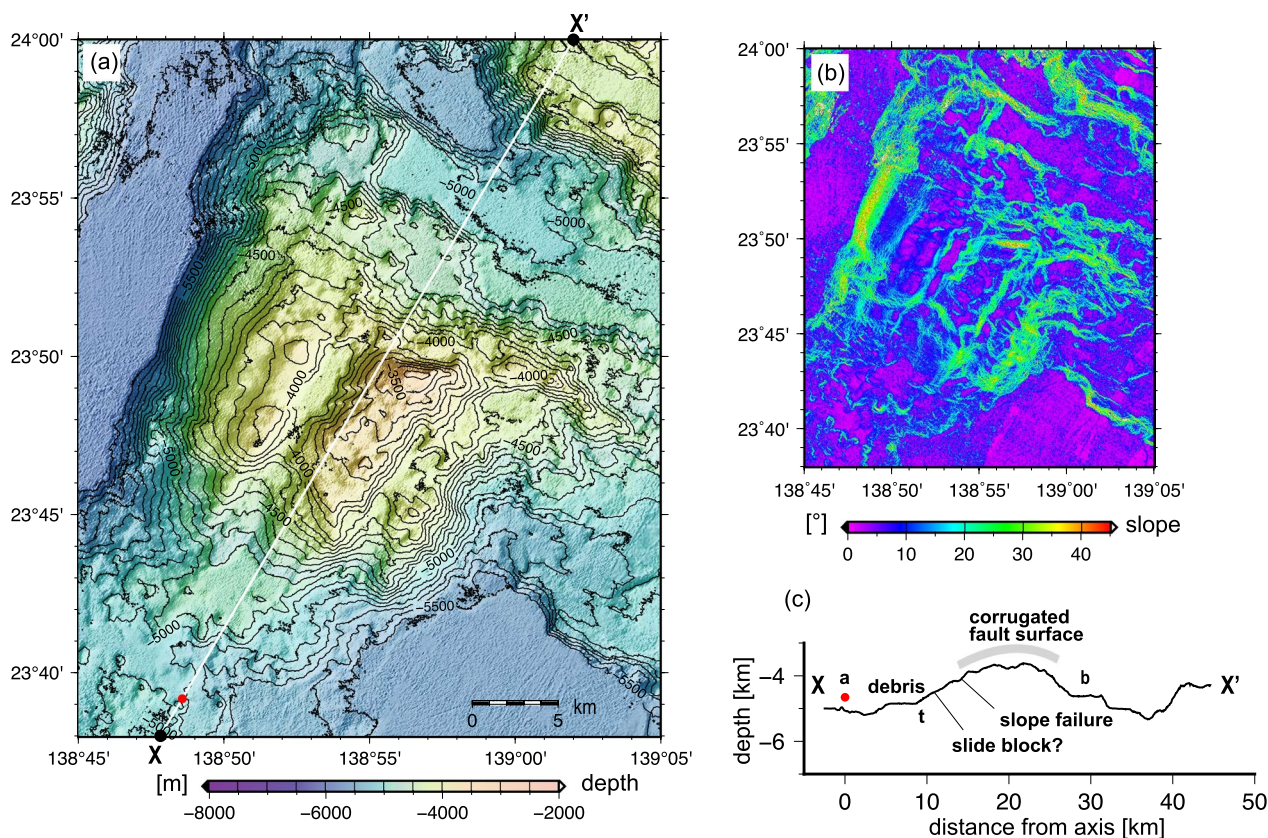


Fig. 3 **a** Close-up view of the Mado MM OCC. The contour interval is 20 m. **b** Distribution of maximum slope magnitude. **c** Bathymetry profile across the Mado MM OCC. The location of the profile is shown in **a**. **a**: axis, **t**: termination, **b**: breakaway

direction and that the spreading process cannot be interpreted as a typical “rigid” plate movement. The far off-axis area, north and northeast of the Mado MM OCC, is enigmatic, and the thick sediment makes it difficult to recognize the basement morphology. However, this sedimented area is anomalously deep compared to the neighboring abyssal hills. Some circular and elongated topographic highs that are considered to be derived from post-spreading volcanism have disturbed the original segment structure (Fig. 2b).

4.2 Age dating

During our four cruises and on one previous cruise in 2007, rock samples were collected using dredge hauls and HOV dives on and around the Mado MM OCC (Basch et al. 2020; Akizawa et al. 2021; Hirauchi et al. 2021; Sen et al. 2021). Gabbroic rocks and serpentinized peridotites were dominant over the OCC, and dolerite, basalt, rodingite, amphibolite, and schist samples were also collected (Fig. 2a, Additional file 4: Table S1). One dredge was conducted at the NTO massif and one at the elongated OCC east of the Mado MM OCC in the previous cruise, where we recovered peridotites (Fig. 2a).

To determine the age of the Mado MM OCC formation, nine gabbroic samples were chosen for zircon U–Pb geochronology (Table 1). Samples were collected with dredge hauls during the R/V *Hakuho-maru* KH-18-2 cruise (D05 and D12) and by HOV *Shinkai 6500* during

the R/V *Yokosuka* cruises YK18-07 (Dive #1515), YK19-04S (Dive #1536), and YK20-18S (Dive #1569). Onboard descriptions of the samples analyzed ranged from altered coarse-grained gabbro (6K1515-R14), olivine gabbro (6K1536-R14a, -R18, -R20, and D05-101A), gabbro mylonite (6K1569-R04, -R06), and diorite (D12-401). Sample D05-101B is a felsic domain of the gabbro sample -101A. More detailed petrography and geochemistry of the gabbroic samples analyzed will be undertaken in separate studies.

Most of the zircon crystals and fragments separated from gabbroic rocks have euhedral to subhedral, equant to stubby morphologies of ~30 to several hundred microns long. Zircon U–Pb age analyses were conducted using the laser ablation inductively coupled plasma mass spectrometry system at the National Museum of Nature and Science, Japan. The reported ages for each sample (with 95% confidence intervals) in Fig. 4 are weighted means of ^{207}Pb -corrected $^{206}\text{Pb}/^{238}\text{U}$ age data ($n=5\text{--}22$ analyses per sample). Details of sample preparation and analytical procedures can be found in Additional file 1: S-1, along with data on zircon isotope compositions and ages.

Among the samples analyzed, six samples (6K1515-R14, 6K1536-R14a, -R18, -R20, 6K1569-R06, and D05-101A) yielded well-grouped weighted mean ages ranging from 11.74 ± 0.61 Ma to 12.96 ± 0.30 Ma (Fig. 4). The remaining three samples (6K1569-R04, D05-101B, and D12-401)

Table 1 Sampling locations and mineralogy of the studied samples

| Cruise | Dredge/ Dive number | Sampling location (WGS84) | Depth (mbsl) | Sample name | Rock type | Mineralogy | $^{238}\text{U}/^{206}\text{Pb}^*$ age (this study) | Reference | Map key | |
|----------|---------------------------|-----------------------------------|--------------|-------------|----------------------------------|----------------------------------|---|---------------------|---------|----|
| KH-18-2 | D05 | 23° 51.7310' N 138° 57.8930' E | 4522 | D05-101A | Varitextured gabbro | Pl, Cpx, Amp, Ol | 12.96 ± 0.30 Ma | 1, 2 | 6 | |
| | | | | D05-101B | Hybridized gabbro | Pl, Cpx, Amp, Ol, Ox | <i>13.12 ± 0.37 Ma</i> | 1, 2 | 6 | |
| | D12 | 23° 49.3060' N 138° 47.6350' E | 5403 | D12-401 | Diorite | Pl, Amp | <i>13.17 ± 0.71 Ma</i> | | 7 | |
| YK18-07 | 6K1515 | 23° 50.4372' N 138° 48.3942' E | 5073 | 6K1515-R14 | Oxide gabbro | Pl, Cpx, Ox, Amp | 12.54 ± 0.56 Ma | 1, 2 | 3 | |
| YK19-04S | 6K1536 | 23° 49.7226' N 138° 56.6931' E | 3608 | 6K1536-R14a | Coarse-grained olivine gabbro | Pl, Cpx, Ol, Amp | 12.70 ± 0.33 Ma | 1 | 9 | |
| | | | | 3540 | 6K1536-R18 | Coarse-grained olivine gabbro | Pl, Cpx, Ol, Amp, Ox | 11.74 ± 0.61 Ma | 1, 2 | 9 |
| | | | | 3498 | 6K1536-R20 | Mylonitic oli- vine gabbro | Pl, Cpx, Amp, Ol, Ox | 12.83 ± 0.41 Ma | 1 | 9 |
| YK20-18S | 6K1569 | 23° 53.3793' N 138° 49.0433' E | 5713 | 6K1569-R04 | Olivine gabbro | No thin section | <i>13.15 ± 2.27 Ma</i> | 2 | 13 | |
| | | | | 5713 | 6K1569-R06 | Oxide gabbro | No thin section | 12.22 ± 0.37 Ma | 2 | 13 |

Pl, plagioclase; Cpx, clinopyroxene; Amp, amphibole; Ol, Olivine; and Ox, Fe-oxide

Reference 1, Basch et al. (2020); 2, Akizawa et al. (2021)

Ages in italic are for reference only

Pb* indicates the radiogenic portion

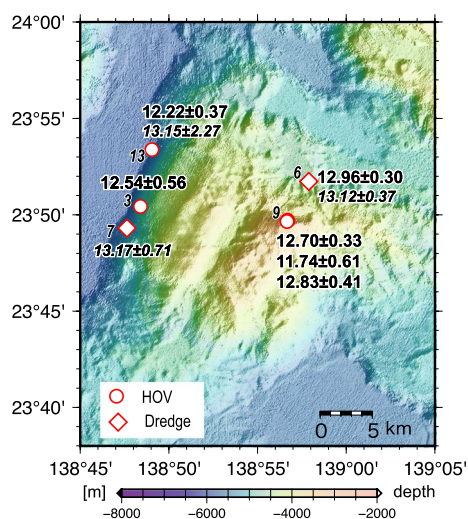


Fig. 4 Weighted means of ^{207}Pb -corrected $^{206}\text{Pb}/^{238}\text{U}$ age data. Less reliable data due to a small number of analyzed zircons are in italic. See Additional file 4: Table S1 for the map keys

are less reliable (shown in italic in Fig. 4) because of the small numbers of analyzed zircons ($n < 6$). However, they fall within the age variation of the other samples (Fig. 4).

We cannot know the sample occurrence for dredge samples (diamonds in Fig. 4), and these samples are possibly ex situ. During the HOV dives (circles in Fig. 4), it appears that the samples are rubbles on the slope; hence the possibility of the ex situ origin of these samples cannot be completely ruled out. However, since the outcrops were observed just above or upper slope of each sampling point, the collected samples, even if they had shifted from their original positions at outcrops, can be considered as in situ. Moreover, the tracks of HOV dives were across the remnant transform fault wall or the corrugation, and the shift of rubbles from the original positions at outcrops, even if it occurred, should have been parallel to the isochrons, not toward the axis. Therefore, we consider that the determined age represents the age of the detachment surface at each sampling point.

4.3 Magnetic anomalies

The deskewed magnetic anomalies and equivalent magnetization distribution are shown in Fig. 5a and b. The magnetic anomaly pattern is generally consistent with the morphological features. The western edge of the survey area at 138° 20' E, where the N–S trending abyssal hill pattern develops, is characterized by N–S extending strong positive anomaly zone. This suggests the occurrence of east–west seafloor spreading in the first half of the basin formation. Previous studies (Sdrolias et al. 2004; Okino 2015) have recognized the similarly strong and broadly positive magnetic anomaly in

the northern extension of this area and have identified this anomaly as Chron 6 (18.748–19.722 Ma). The magnetic anomaly lineation rotates anticlockwise east of 138° 30' E, indicating the change in the spreading direction. The anomaly pattern is not easy to identify, which is partly due to the fine segmentation of the spreading axis and the complex evolution process before and after the cessation of the spreading.

The southwestern flank of the Mado segment shows a relatively clear magnetic reversal pattern, comprising magnetic lineation of approximately 20 km-long in length. These short lineations change their trend gradually from N175° E at 138° 30' E to N128° E at the axis. These anomalies enable us to identify their chrons, as described later. The general magnetic anomaly pattern looks similar in the southwestern flank of the neighboring segment, suggesting the occurrence of continuous crust accretion, at least on the southwestern side of the spreading axis during the second half of the basin history. Contrary to the relatively well-ordered magnetic anomaly pattern, the seafloor spread to the northeast shows an ambiguous and complex magnetic anomaly pattern. The NW–SE trending stripes can be partially observed, but the anomalies are irregularly distributed. This likely suggests a more complicated crustal structure, the effect of thick sediment cover, and post-spreading volcanism.

The Mado MM OCC is characterized by a wide zone of positive magnetic anomaly from the termination to 14 km off-axis, comprising more than half of the OCC. This positive zone is wider than the magnetic lineation on the southwestern side. The repeated negative and positive stripes can be recognized near the breakaway zone and the northeastern off-axis. The NTO massif at the ridge-transform-ridge intersection shows weak magnetization, which is consistent with its non-volcanic origin.

Figure 5a also shows the loci and strike of the magnetic boundaries derived from the vector magnetic anomaly analysis. This generally builds on the observations of total magnetic anomalies. The length of the red bar is proportional to the cosine of the boundary inclination, and the length of the thin black cross bar indicates the angular standard deviation of the boundary strike. The magnetic boundary can be caused by magnetic reversal, change of magnetization strength, and topographic change of the magnetized layer. The systematic change in boundary strike in the southwestern off-axis area indicates the gradual rotation of the spreading axis in the latter half of the basin formation. Some boundaries exist on the Mado MM OCC, but the pattern is not well organized. The high standard deviation and large boundary inclination suggest the three-dimensionality of the magnetic body (Seama et al. 1993). The NTO massif southeast of

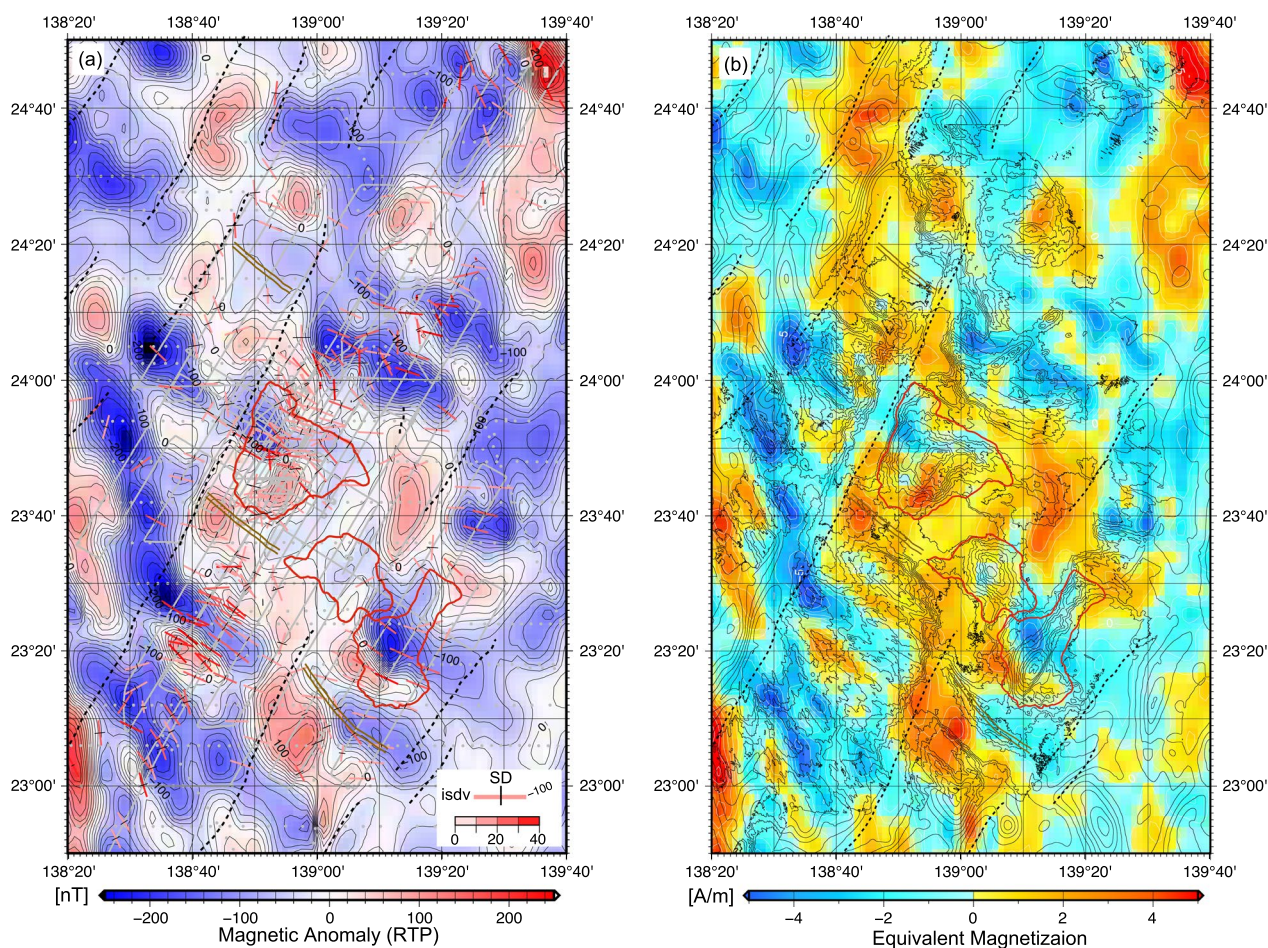


Fig. 5 Magnetic features of the surveyed area. **a** Reduced to pole (RTP) magnetic anomalies and the loci and strike of magnetic boundaries with ISDV magnitude and standard deviation (red bars with black crossing lines). The data points are shown in gray. **b** Equivalent magnetization of the seafloor. White lines show 1 A/m-contours of magnetization. Bathymetry contours (black, 200 m interval) and major morphological features are plotted

the Mado MM OCC is not accompanied by any magnetic boundaries.

To identify the magnetic anomalies and to deepen our knowledge of the spreading history, we first conducted a simple forward modeling of the magnetic profiles across the Mado segment (Fig. 6a). Two profiles were modeled by using the reduced-to-the-pole magnetic anomaly, in which Profile A was across the Mado MM OCC, and Profile B was located south of the OCC. The length of the profiles selected was approximately 320 km, stretching ~180 km and 140 km on the northern and southern flanks, respectively. We assumed that there was a 500 m-thick single source layer with constant 3 A/m magnetization, draping the bathymetric profile. The conditions of constraint for the modeling were (1) the identification of N-S trending strong positive anomaly at 138° 20' E as Chron 6 following the previous studies, and (2) the results of rock age dating, that is, 12–13 Ma all

across the Mado MM OCC. Figure 6b shows the result of the forward modeling. This model includes two spreading phases, namely symmetric spreading with a half rate of 22 mm/yr. until 16 Ma, symmetric slower spreading with half rate of 11 mm/yr. between 16 Ma and 12.5 Ma. We identified magnetic chrons from C5Er (18.7 Ma) to C5Ar (13.0 Ma-) in the southwestern off-axis flank. The same chrons were also identified in the northeastern off-axis flank, although the pattern matching was not as well defined as on the southwestern off-axis flank.

These preliminary analyses indicate a reduction in the spreading rate in the final stage. However, the inconsistency of the calculated and observed profiles is still existed, especially on the northeastern flank where the Mado MM OCC is hosted. This inconsistency has indicated that there was a fluctuation in the spreading rate and/or a more complex magnetic structure. We then applied the methods of Zhou and Dymant (2022) to

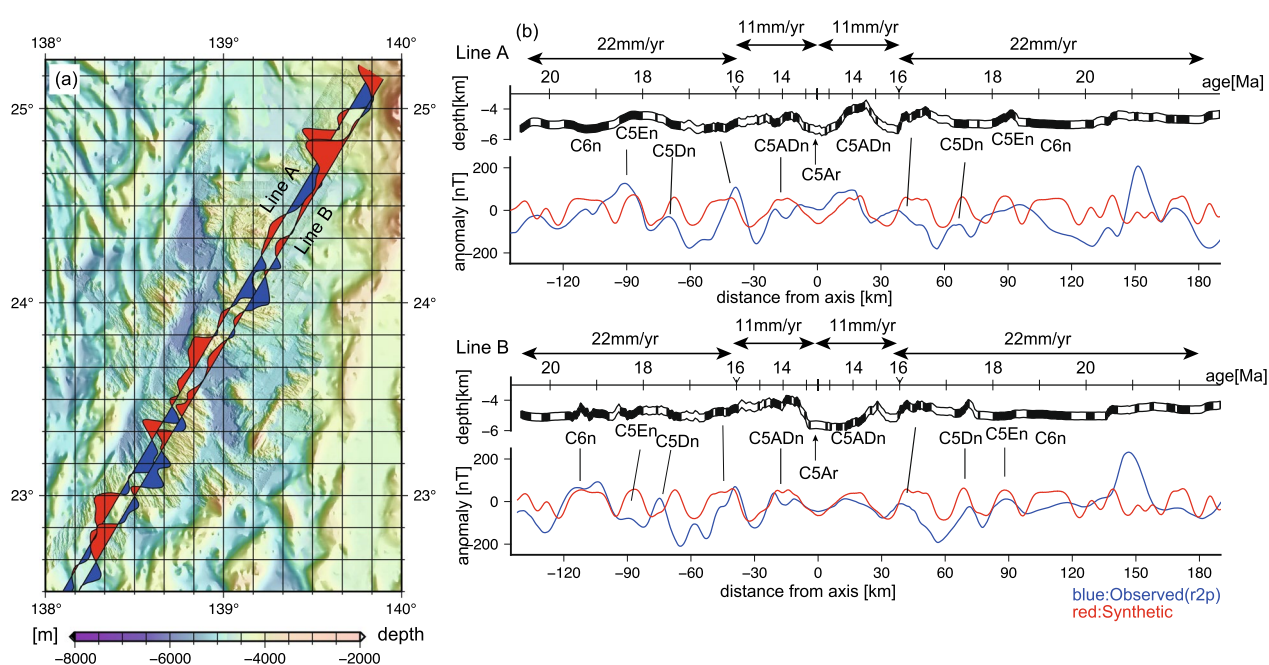


Fig. 6 Simple one-layer forward modeling of the magnetization structure across the Mado segment. **a** Wiggly plot of RTP magnetic anomalies along two lines on the bathymetry map. **b** Magnetization block model (top) and observed (blue) and synthetic (red) profiles along Lines A and B

model the lithospheric structure and evolution. In this detailed forward modeling, a 3 km thick magnetized layer was assumed to comprise a maximum 500 m thick basalt layer, a 1500 m thick gabbro layer, and a 1000 m thick peridotite layer. We simulated the gradual decrease in thickness from the center to the end of each magmatic crust to smooth transit to the tectonic crust. The basalt layer bears a remanent magnetization of 3 A/m, the underlying gabbro layer bears a remanent magnetization of 1 A/m, and the peridotite layer bears an induced magnetization of 0.2 A/m. Intrusive gabbro bodies beneath the detachment footwall obtained a higher remanent magnetization of 2 A/m because the faster cooling rate resulted in a higher degree of fractionation. We set a remanent magnetization of 0.5 A/m for the exposed peridotite during tectonic spreading episodes, although the value can vary widely depending on the degree of serpentinization.

The modeling results (Fig. 7b) show an acceptable fit between the synthetic and observed magnetic anomalies along the two profiles. The seafloor spreading of the two profiles was dated to ~ 22 Ma to the north and ~ 20 Ma to the south. The intervals of the magnetic isochrons were adjusted to better fit the synthetic and observed magnetic anomalies with a calculation of half-spreading rates in each episode. There was generally a decrease in the spreading rate from 22 to 11 mm/yr. at ~ 16.0 Ma, and seafloor spreading finally stopped at ~ 11.9 Ma. The

Mado MM OCC was formed during ~ 12.2 – 14.1 Ma on Profile A, during which time the seafloor spreading showed a significant asymmetry with a half-spreading rate of 34 mm/yr. on the hosted northern flank compared with a 5 mm/yr. on the southern flank.

The magnetic anomaly pattern cannot straightforwardly be interpreted because of the geological complexity of the OCC, and our forward modeling results show one possibility. We will discuss this issue later.

4.4 Gravity anomalies

The result from the gravity anomaly analyses is consistent with other datasets. Figure 8 shows the free-air (Fig. 8a) and mantle Bouguer anomalies (MBA) (Fig. 8b) and the estimated crustal thickness (Fig. 8c) and density variation (Fig. 8d) assuming the constant density contrast and constant crustal thickness, respectively. The Mado MM OCC and the NTO massif are accompanied by strong positive MBA, suggesting high-density material in the shallower part. The western edge of the survey area also shows a positive MBA. This may be related to the change in the spreading stage, but we have not explored this further in this study in the absence of detailed bathymetry data.

The Mado MM OCC shows a significant MBA value of ~ 20 mGal larger than the surrounding area. The large MBA area extends southeastward, out of the domed high, encompassing the entire Mado segment. This value corresponds to a 3.4 km decrease in magmatic crust or a

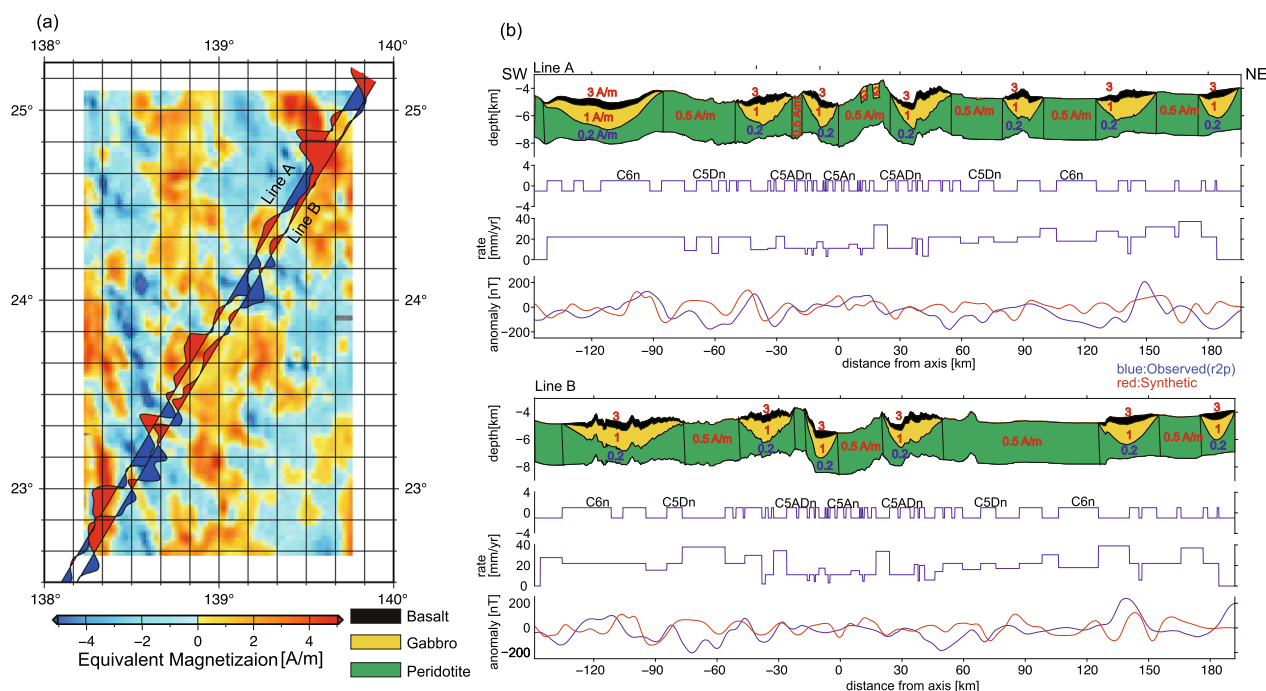


Fig. 7 Three-layered forward modeling of the magnetization structure across the Mado segment. **a** Wiggly plot of RTP magnetic anomalies along two lines on the equivalent magnetization map. **b** Lithology model with assumed magnetization (top) and observed (blue) and synthetic (red) profiles along Lines A and B

270 kg/m³ decrease in density. The weaker positive MBA area extends to the eastern part of the Mado segment, where the seafloor is relatively deep and flat without any corrugation. The NTO massif also shows a positive MBA as large as the Mado MM OCC. In contrast, the elongated OCC at 23° 20' N, 139° 10E in the eastern segment does not show a significantly positive MBA. This is likely consistent with the clear magnetic anomaly lineations over this OCC, suggesting the presence of a thicker magmatic layer.

Another positive circular MBA is observed at 22° 55' N, 139° 07' E. This anomaly likely corresponds to the bathymetric high (Fig. 2a) immediately southwest of the neighboring rift axis.

5 Discussion

5.1 Detachment faulting at Mado MM OCC

The geophysical characteristics described in the previous chapter and the rock samples collected (Basch et al. 2020; Akizawa et al. 2021; Hirauchi et al. 2021; Sen et al. 2021) have indicated that the Mado MM OCC is a result of tectonic-dominant extension along a detachment. The Mado MM OCC is located at the inside corner of the relict ridge-transform intersection. The across-axis length is ~25 km, which is a typical horizontal scale for other OCCs along slow-spreading ridges. The bathymetry profile (Fig. 3c) shows a single dome-like shape with

a relatively steeper slope on the breakaway side. Continuous corrugations develop at ~10 km on the flat top of the dome.

The gabbroic rocks and serpentinized peridotite collected from the entire OCC suggest that the lower crust/upper mantle materials are exposed at the shallow subsurface. Our gravity analysis showing a high MBA for the Mado MM OCC has supported this idea (Fig. 8b). A more in-depth discussion about the crustal thickness is difficult especially in the absence of seismic data. However, the equivalent crustal thickness from gravity analysis assuming standard density contrast between crust and mantle could have dropped by up to 50% (Fig. 8c). The previous numerical model studies (Buck et al. 2005; Tucholke et al. 2008) suggest that a long-lived detachment develops when the melt supply rate M is ~0.5. The 50% reduction in the estimated crustal thickness does not necessarily mean that M is 0.5 because of the trade-off between the thickness and the density and of the complex lithology, but it suggests that the melt supply fluctuated and was reduced during the OCC formation.

The higher MBA zone extends southeast of the OCC and along the western relict transform fault to the north, where no corrugation is observed. The MBA is relatively low northeast of the OCC, but it may reflect the post-spreading off-axis volcanism (Fig. 2b). The southwestern flank of the Mado segment within ~40 km from the

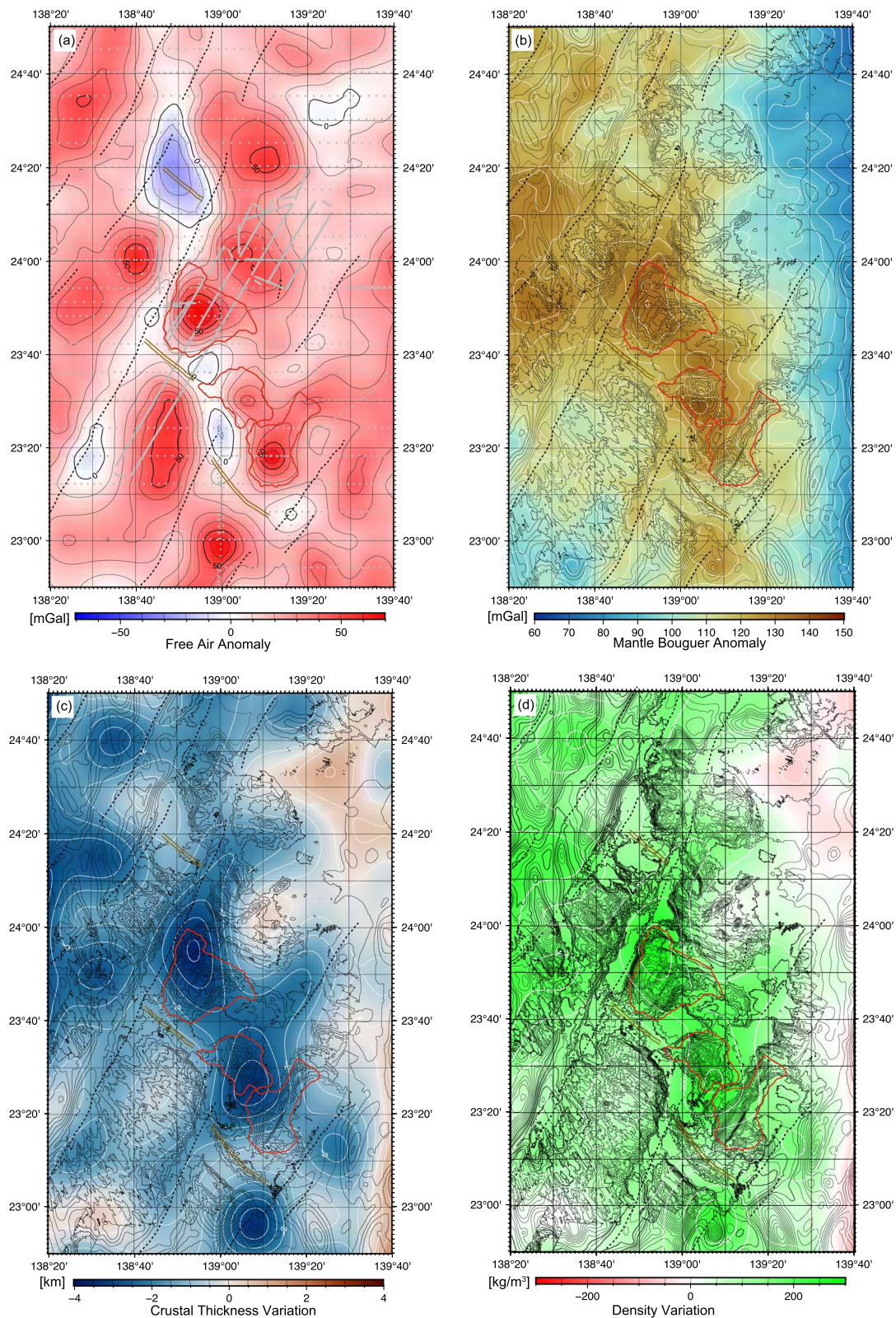


Fig. 8 Gravity features of the surveyed area. **a** Free-air gravity anomalies with contours of 10 mGal intervals. The data points are shown in gray. **b** Mantle Bouguer gravity anomalies. White lines show 10mGal-contours. **c** Inferred crustal thickness variation. White lines show 0.5 km-contours. The reference crust thickness is 6 km. **d** Inferred density variation. White lines show 50 kg/m³-contours. In **b**, **c**, and **d**, bathymetry contours (black, 200 m interval) and major morphological features are plotted

axis shows a relatively thinner crust than the far off-axis (Fig. 8c). This area shows a regular abyssal hill morphology and was formed in the period when the spreading rate was halved (Fig. 6). These observations suggest that the melt supply was generally declining as the spreading rate had decreased and that the transition from the typical accretion style forming well-ordered abyssal hills to the detachment faulting with corrugations could result from a modest variation in melt supply.

The lineated magnetic anomalies in the southwestern off-axis of the Mado segment (Fig. 5), where the well-ordered abyssal hill develops, record the spreading history, whereas the anomalies over the Mado MM OCC cannot be explained by a simple normal-reverse model (Fig. 6). Xu and Tivey (2016) investigated the magnetic polarity reversals over the Kane Megamullion using near-bottom magnetic field data collected by HOV. They found the large variation of magnetic anomaly identified as the magnetic polarity boundaries in the scarp, suggesting that the gabbros and mantle peridotites potentially record a magnetic reversal history. Sato et al. (2009) analyzed the scalar and vector magnetic field over the 25°S OCC near the Rodrigues Triple Junction in the Indian Ocean. The 25° S OCC is weakly magnetized and records a polarity boundary that is consistent with the magnetic lineation around the OCC. Baines et al. (2008) also reported that the magnetic lineation age correlates well with the U–Pb zircon age in the Atlantis Bank. These studies indicated that OCCs could record the spreading history, but this is not true for all OCCs. Generally speaking, the magnetic structure of OCCs is much more complex because of the geological complexity in the original lithology and the deformation associated with the detachment faulting.

The first factor in the complexity of the magnetization of OCCs is the inherent heterogeneous lithology. Hayman et al. (2011) analyzed the aeromagnetic data over the ultraslow Mid-Cayman Spreading Center (MCSC) and concluded that the magnetizations were heterogeneous and quite patchy, with a rough correlation with bathymetry and lithology. The most prominent OCC along the MCSC, the Mount Dent displays a relatively low level of magnetization, reflecting the predominance of gabbros and peridotites. Zhou and Dymant (2022) interpreted the variability of magnetic anomalies at the Southwest Indian Ridge using the intruded gabbro bodies on the footwall of the detachment faults. Our three-layer forward model (Fig. 7) uses the similar methodology and tried to model the observed profile by heterogeneous crust with frequent gabbro intrusions. If serpentinized peridotite occupies a substantial proportion of the OCC, induced magnetization also may play an essential role in OCC magnetization. However, quantitative estimation is

rather difficult because the magnetic susceptibility predominantly depends on the degree of serpentinization, which varies in an OCC. In our magnetic structure model (Fig. 7b), the peridotite body is assumed to have 0.5 A/M magnetization, but other values can also be applicable. Our result is one possible interpretation of the observation, but it is not a unique solution.

Other factors also influence the magnetization of OCCs and make the variable magnetic anomaly pattern. The doomed surface of OCCs is a result of flexural rotation along the fault (Buck 1988), causing the change in inclination. Mallows and Searle (2012) analyzed the deep-tow magnetic data across the OCC1320 and OCC1330 along the MAR and showed that the observed magnetic profile could be effectively modeled by weaker magnetization and 45° rotation for the OCCs. A similar conclusion was obtained by Searle et al. (2019) using magnetic data obtained from an autonomous underwater vehicle. These studies are based on higher spatial resolution magnetic and bathymetry data by near-bottom surveys. Although our surface magnetic data do not have enough resolution to discuss the detachment rotation, disordered magnetic anomalies may reflect the rotation effect as well as the heterogeneous lithology. The footwall rotation of the Atlantis Massif was proposed using paleomagnetic data of the IODP (Integrated Ocean Drilling Program) core samples (Morris et al. 2009; Pressling et al. 2012) that instead, the magnetic record of the OCCs is influenced by the flexural rotation of the detachments.

Moreover, the hypothesis that the surface of OCCs shows a sequential unit is not always correct. The transposition of units, incorporation of hanging wall material into the footwall of the detachment fault and other surface processes such as erosion and mass wasting (e.g., Escartín et al. 2022) hinder the straightforward interpretation of observed magnetic anomalies. The chaotic magnetic boundaries over the Mado MM OCC derived from our vector magnetic analysis (Fig. 5a) also support the heterogeneous structure of the detachment fault, both inherent and subsequent deformation.

The complexity of the magnetic structure of the OCCs prevents us from obtaining definitive magnetic ages, but the identification of lineated magnetic anomalies in the conjugate seafloor can provide an essential constraint of OCC formation. The magmatic crust in the southwestern flank of the Mado segment comprised well-ordered abyssal hills from chron C6 to C5Ar (Fig. 6b). The half-spreading rate decreases from 22 to 11 mm/yr. around 16 Ma, and the Mado MM OCC was considered to form under this final, slower (close to ultraslow) spreading environment. The northeastern off-axis area that was formed before the Mado MM OCC formation shows unclear abyssal hills, and the overprinted volcanic constructions

deeper axial basin is located south of the massif and the eastern corrugated seafloor described below appears to be continuous to the massif.

The NTO massifs along the MAR are generally located within the 2nd-order discontinuities rather than at the 1st-order discontinuities, that is, transform faults. Second-order discontinuities along slow-spreading ridges are often oblique to the plate motion, and the resultant trans-extension causes a magma-poor extension along a detachment. In the case of the Mado segment and the surroundings, we recognize that short ridge segments are offset by relict transform faults because the discontinuity is narrow, generally stable, and long-lived. However, the fracture zones, traces of transform faults, have shown a characteristic sigmoidal curve (Fig. 2). This geometry indicates the continuous counterclockwise rotation of the spreading direction in line with that of the Parece Vela Rift (Kasuga and Ohara 1997; Spencer and Ohara 2014). Meanwhile, the rigid plate motion on a single Euler pole should produce a set of parallel fracture zones along

small circles. This rotation causes the shortening of the ridge segment (Spencer and Ohara 2014), which likely enhances the complex, locally oblique geometry of the ridge-transform intersections. The Mado NTO massif may be located at a 1st-order discontinuity in terms of its appearance, but the unusual kinematics may have caused a magma-starved spreading at the segment discontinuity.

East of the Mado segment, a set of corrugations extends on the northeastern side of the remnant rift (Fig. 2). Although the corrugations are prominent and continuous, the seafloor does not have a single, dome-like structure. At least three corrugations were recognizable. The most prominent ~40 km long corrugation extended in a flow-line direction, where three peaks could be identified along the corrugation (Fig. 10b). This may indicate the potential for multiple detachments. The high MBA area continues from the NTO massif to this long corrugation (Fig. 8b), and there are two short corrugations located between them. The gravity anomalies suggest that higher-density material is present in the shallow

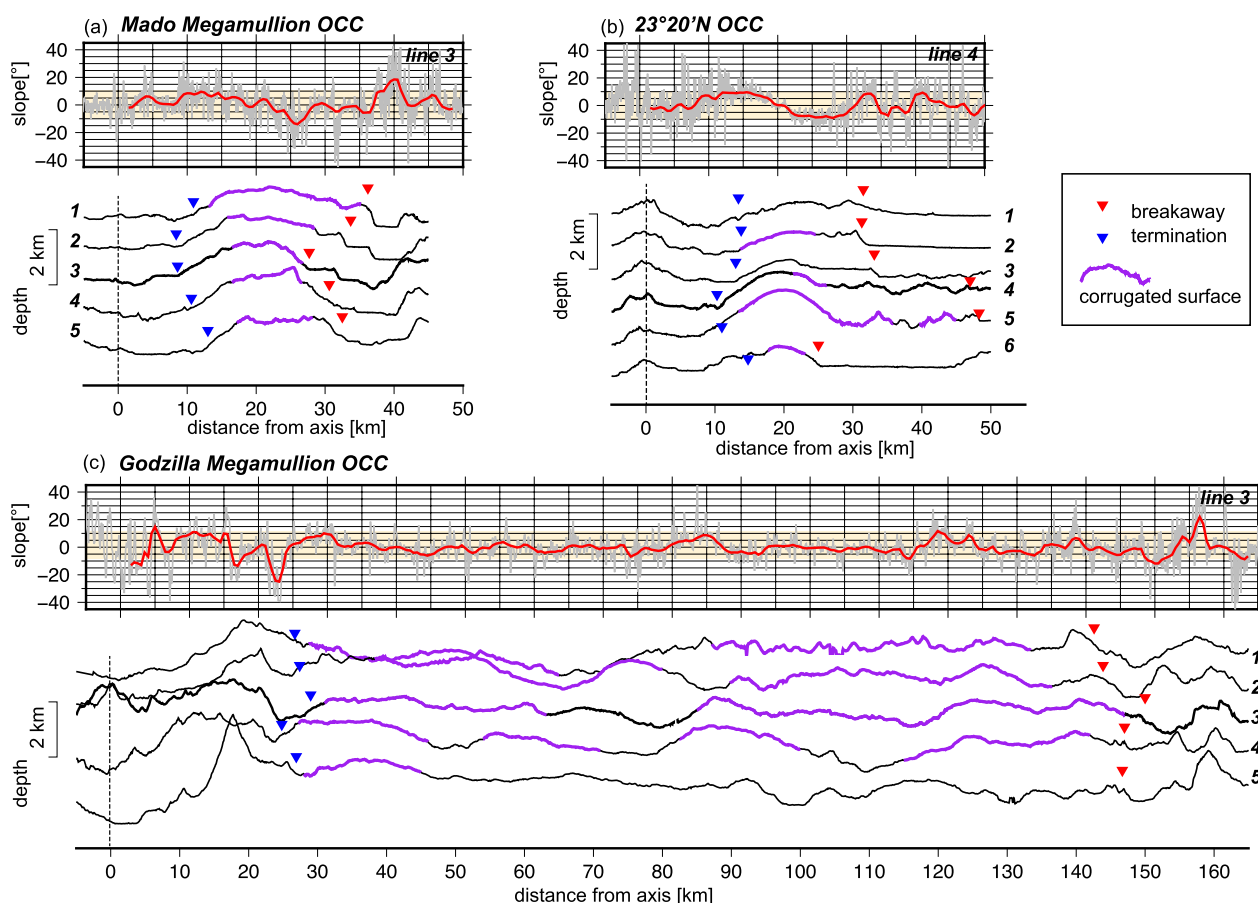


Fig. 10 Slope and depth profiles across three OCCs in the same scale. The locations of the profiles are shown in Fig. 11 a, b and e. Raw slope profiles are shown in thin black lines, and 3 km-slope Gaussian moving averages are in red. The loci of termination (hanging wall cutoff) and breakaway of detachment faults are plotted on depth profiles. The corrugated areas are also shown. **a** Mado MM OCC, **b** 23° 20' N OCC, and **c** Godzilla MM

subsurface, possibly an intermittent gabbro intrusion, but no rock samples have been collected here.

A small, circular MBA high was observable along the fracture zone at 22° 55' N, 139° 07' E (Fig. 8b). We do not have multibeam bathymetry here, but the public bathymetry data of 30'' resolution has indicated the existence of a conical high. We cannot reliably calculate the MBA and cannot investigate its detailed morphology on it. However, this structure is a candidate for being another OCC that has developed at the remnant axis.

These observations suggest that the final stage of the back-arc opening in this area was generally magma-poor, and detachment faulting likely played a key role.

5.3 Magma-starved spreading at the final stage of back-arc opening

In the previous section, we have shown that detachment faulting is the main process of the back-arc opening at the final stage in the Mado and neighboring segments. Although many OCCs have been reported along global

ridge systems ranging from ultraslow (e.g., Searle et al. 2003; Cannat et al. 2006; Hayman et al. 2011; Sauter et al. 2013; Grevenmeyer et al. 2018; Haughton et al. 2019; Corbalán et al. 2021), slow (Cann et al. 1997, 2015; Tucholke et al. 1998, 2008; Ranero and Reston 1999; Smith et al. 2006, 2014; Escartín et al. 2008) to intermediate (Okino et al. 2004) rates, the reports from back-arc spreading systems are highly limited. All of the back-arc basin OCC studies have been conducted in the Philippine Sea.

Many OCCs are distributed along the Parece Vela remnant back-arc rift (PVR, Fig. 11). The rift axis is highly segmented and hosts anomalous massifs, although the well-ordered abyssal hills are dominant in the far off-axis. The Godzilla Megamullion (GMM), which is a large and well-studied OCC, is located at 15° N (Fig. 11e). Here, 125 km-long corrugated surfaces are exposed (Fig. 10c) and have developed across the entire segment (Ohara et al. 2001; Harigane et al. 2008, 2010, 2011b, 2011a, 2019; Tani et al. 2011; Loocke et al. 2013; Spencer and Ohara 2014; Ohara 2016, 2021). North of the GMM

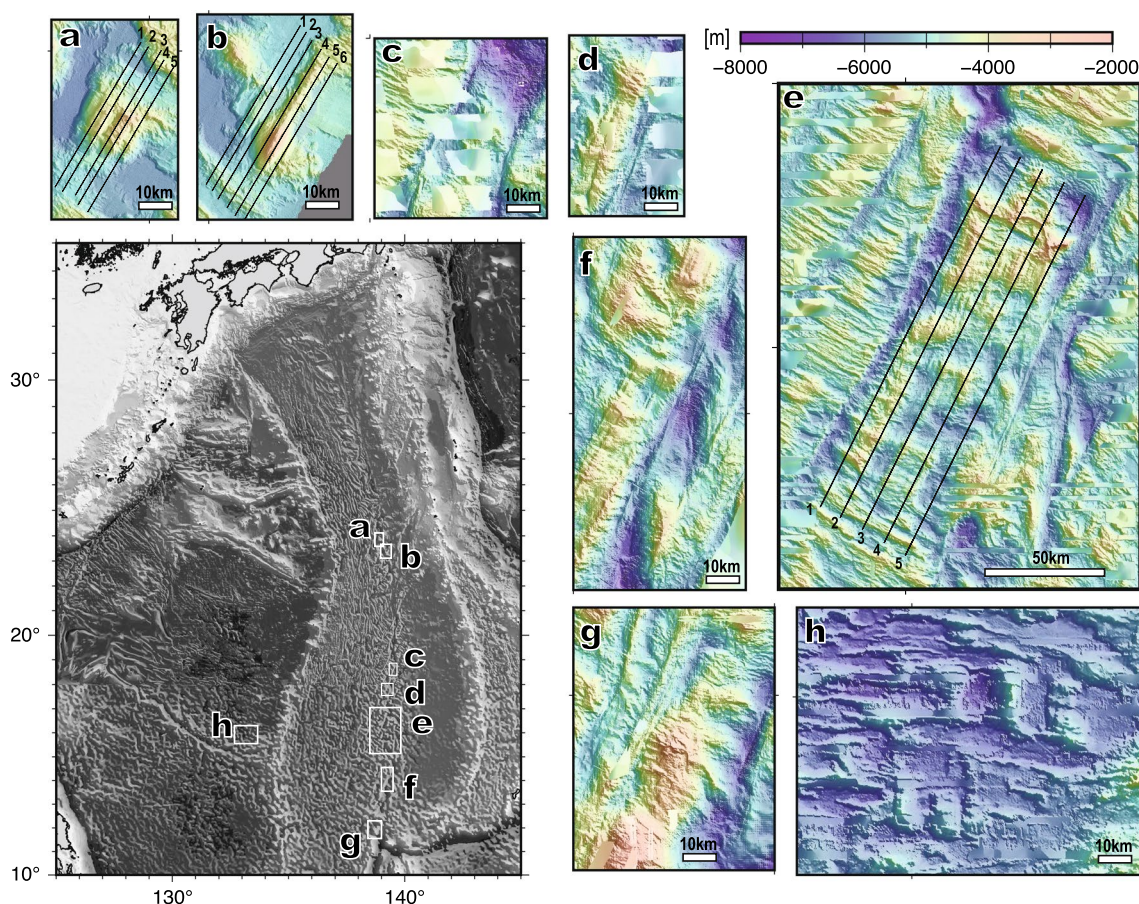


Fig. 11 Wide-spread OCC-like structures along remnant spreading centers in the Philippine Sea. **a** Mado MM OCC, **b** 23° 20' N OCC, **c** Parece Vela Rift S1, **d** Parece Vera Rift S2, **e** Godzilla MM, **f** Southern Parece Vela Rift, **g** Southernmost Parece Vela Rift, **h** eastern CBF Rift. The Godzilla MM (Fig. 11e) is shown on a different scale

segment, two segments host massifs immediately southwest of the remnant rift axis (Fig. 11c and d). The surface of these massifs is relatively smooth without clear corrugations, and peridotite samples have been reported (Ohara et al. 2003; Ohara et al. 2011). These massifs can be categorized as “smooth seafloor” (Cannat et al. 2006), which has indicated a much melt-starved condition. The area south of the GMM has not been well studied, but the limited multibeam bathymetry has indicated that the OCC-like structures with corrugations have developed adjacent to the remnant rift axis (Fig. 11f). A corrugated dome structure is located at the southwestern flank of the remnant rift (top of Fig. 11f), and another set of corrugations seem to extend more than 50 km far off-axis. Gong et al. (2022) have reported the exposure of gabbroic rocks and altered peridotites at the southernmost PVR near the junction of the Yap Trench. Their samples were collected from the topographic high without any clear corrugations (Fig. 11g).

The widely distributed OCCs and OCC-like structures along the remnant back-arc spreading axis indicate that the detachment faulting was dominant at the end of the back-arc spreading over the entire PVR. In the process of reaching this final stage, the spreading direction and rate have changed. The general pattern is as same as that of the Shikoku Basin, with the east–west spreading in the first half, and then, the spreading direction gradually changes to a NNE–SSW ~ NE–SW direction with rift axis segmentation. The average half-spreading rate is estimated to be as 40–50 mm/yr. in the east–west spreading stage (26–18.7 Ma) and decreases to ~30 mm/yr. (Okino 2015) in the later stage before the GMM formation. Tani et al. (2011) investigated the development of the GMM using the zircon age dating of the gabbroic samples collected and found a constant of 25.4 mm/yr. spreading across the entire GMM from 13 to 7.9 Ma (Fig. 9). The bathymetric profile and the variation in seafloor slope (Fig. 10c) have shown that the large GMM comprises three domed highs, suggesting multiple occurrences of detachment faulting. Even if the information on the denudation rate of each detachment was insufficient, the repeated detachment faulting caused pronounced and constant spreading over the long GMM. Unfortunately, there are no age data on the conjugate side, and we cannot know if the spreading was asymmetric or not. The decrease in spreading rate in the later stage is common in both the Shikoku and Parece Vela Basins. However, the duration of the final tectonic-dominant phase is different. The GMM suggests that the melt-poor extension continued at slow rate over six million years, whereas the Mado MM OCC was formed over approximately one million years after further reduction of spreading rate (Figs. 6 and 9).

Another group of OCCs has been recognized in the northern off-axis of the eastern part of the CBF Rift (Fig. 11h). The CBF Rift is a remnant spreading center of the West Philippine Basin, alternatively known as the Central Basin Spreading Center (Okino and Fujioka 2003). The origin of this basin is still debated, but it formed from Eocene to Oligocene time (Hilde and Lee 1984; Fujioka et al. 1999; Deschamps et al. 1999, 2002; Deschamps and Lallemand 2002; Okino and Fujioka 2003; Sasaki et al. 2014). The magnetic lineation has indicated that the basin extended in a NE–SW direction in the early phase and the spreading direction then rotated 100° clockwise to a north–south direction, and the axis became segmented in the later phase (Deschamps et al. 1999; Deschamps and Lallemand 2002; Okino and Fujioka 2003). Several OCCs are densely located at the northern off-axis of the eastern CBF Rift, near the junction of the CBF Rift and the Kyushu–Palau Ridge (Ohara et al. 2015). This OCC area extends across an approximately 70×70 miles area. Each OCC is approximately 10–20 km in extent and is accompanied by N–S trending corrugations on them.

The estimated age and spreading rate are different among previous studies. Early work by Hilde and Lee (1984) has proposed the occurrence of NE–SW spreading from 59 to 40 Ma with a half-spreading rate of 4.4 cm/yr. and N–S spreading rate at 1.8 cm/yr. from 40 to 33 Ma. Deschamps and Lallemand (2002) revised the early stage from 54 to 30 Ma and the late extension episode until 26 Ma. However, Sasaki et al. (2014) have suggested that the age of cessation of spread was approximately 36 Ma, and a change in the spreading rate was not required. Their work is predominantly based on the southern flank of the WPB and does not include the identification of the northern flank where the OCCs have developed.

Inactive back-arc basins have indicated that the back-arc opening continued for approximately 10–15 million years and then ceases opening. The mature stage of the back-arc opening is highly similar to those of the mid-ocean ridge process, although the early stage is influenced by subducted slab and arc magmatism to a greater or lesser degree (e.g., Arai and Dunn 2014). However, to date, the ending process of back-arc formation has not yet been investigated. The common features in the later and final stage of the back-arc basins in the Philippine Sea are the change in spreading direction, the decrease in spreading rate, and the melt-poor, asymmetric detachment faulting at the end. It is a remaining question if the termination of back-arc spreading is a passive response to far-field processes or is triggered by the waning of magmatism. We cannot answer this question with certainty, but the presence of a long detachment along the Parece Vela Rift, such as GMM (Fig. 11e) and the southern one

(Fig. 11f), indicates that the extension can continue over a few million years under magma-poor environment, which likely suggests that the primary control may be the far-field process.

The repeated formation of back-arc basins along some convergent boundaries has been reproduced by 2D thermo-mechanical modeling of subduction by Ishii and Wallis (2022). They have shown that trench retreat during back-arc opening caused a decrease in slab dip and the buckling of the slab, and then, the spreading ceased during the buckling phase. Their model predicted an approximately constant velocity of trench retreat for 5–7 million years which then decreased to zero over five million years or less. The constant velocity of trench retreat likely corresponds to the east–west intermediate spreading stage of the Shikoku–Parece Vela Basin formation and the buckling phase to the later NE–SW slow to nearly ultraslow spreading phase. Their model assumes a two-dimensional structure and does not reproduce the rotation of the spreading direction and its effect on the mantle upwelling. Along the Izu–Bonin–Marina trench, the Pacific Plate subducts obliquely beneath the Philippine Sea. As the trench retreat wanes, there is a decrease in the spreading rate of the back-arc, and the influence of oblique subduction likely caused the northward motion of the arc-side sliver, resulting in the rotation of the spreading direction. This also caused the segmentation of the spreading axis because the spreading axis tends to be located at the existing mantle upwelling zone parallel to the trench. This segmentation likely suppresses the two-dimensional upwelling and accelerates the melt-starved environment.

6 Conclusions

We first reported the geophysical features of the Mado Megamullion (Mado MM) oceanic core complex in the Shikoku back-arc basin, which ceased to open in the mid-Miocene. The Mado MM OCC is located nearby the remnant spreading axis and clearly leaves traces of the final appearance of the back-arc opening. The following conclusions were obtained.

1. The Mado MM OCC shows a typical oceanic core complex morphology with prominent flow-line parallel corrugations on the domed high. The termination is a relatively steep slope, partly deformed by mass wasting, and is continuous to the remnant axial rift valley of the Shikoku Basin. It indicates that detachment faulting played a substantial role at the end of the back-arc spreading.
2. The Mado MM OCC is accompanied by a high positive gravity anomaly, indicating that the lower crust/mantle materials are exposed along a detachment fault. The estimated crustal thickness variation is –3 km, half of the normal 6 km-thick crust. There is a trade-off between the density and structure, but this result is consistent with the idea that the melt supply rate M is approximately 0.5 for the detachment-dominant phase predicted by numerical modeling.
3. The zircon U–Pb ages were determined for nine gabbroic samples collected over the entire Mado MM OCC. All of the analyzed ages cluster around 12–13 Ma and do not exhibit systematic spatial variation over the detachment.
4. The back-arc spreading in the Shikoku Basin comprises former east–west spreading at 30–40 mm/yr. (half rate), and later NE–SW ~ NNE–SSW is spreading at a relatively slow rate. Our magnetic analysis has shown that the spreading rate decreased to 20 mm/yr. at ca. 19 Ma when the spreading direction started to rotate and again reduced to 11 mm/yr. at 16 Ma. The three-layer forward modeling has suggested that the Mado MM OCC formed from 14.1 to 12.2 Ma, which is concordant with the zircon age data from the gabbroic samples. The model has also shown that the spreading rate was higher (~34 mm/yr.) on the detachment side, causing pronounced asymmetric spreading at the initiation of the detachment.
5. Other evidence of tectonic-dominant spreading was also observed near the Mado MM OCC. A non-transform offset massif was also present, which likely developed along another detachment in the nodal basin at the southeastern end of the Mado segment. Another OCC with a corrugated surface potentially indicated a multi-detachment, developing at the neighboring segment to the east. These features were accompanied by a high gravity anomaly and exposure of mantle rocks, which suggested the occurrence of melt-starved, tectonic-dominant spreading in the broader areas.
6. These observations are common features reported along the Parece Vela Rift, the remnant spreading axis of the Parece Vela back-arc basin, and the eastern CBF Rift, the remnant spreading axis of the West Philippine Basin. That is, (1) stable, relatively fast spreading potentially parallel to the trench, (2) the spreading direction rotated, causing the segmentation of the ridge axis, and (3) detachment faulting played a key role at the end of the back-arc opening.
7. In the case of the Shikoku–Parece Vela basins, the spreading rate slowed down in the later phase. At the Mado segment, the spreading rate moreover slowed down immediately before the end of the spreading. The segmentation of the axis and slower spreading rate constricted the stable mantle upwelling and led

to the extensive occurrence of OCC and/or smooth seafloors along the remnant rift axis.

Abbreviations

| | |
|-----|-----------------------|
| OCC | Oceanic Core Complex |
| GMM | Godzilla Megamullion |
| PVB | Parece Vela Basin |
| MAR | Mid-Atlantic Ridge |
| WPB | West Philippine Basin |

Supplementary Information

The online version contains supplementary material available at <https://doi.org/10.1186/s40645-023-00570-2>.

Additional file 1. Supplementary material document for station numbers and detailed methodology of zircon age dating.

Additional file 2. Suppl. Fig. 1. Terra-Wasserburg concordia diagrams and age distribution plots for the zircons analyzed from the samples. Detailed caption is in Additional File 1.

Additional file 3. Suppl. Fig. 2. Representative cathodoluminescence images of zircons analyzed for U-Pb dating. Detailed caption is in Additional File 1.

Additional file 4. Suppl. Table 1. Sampling sites and primary lithology.

Additional file 5. Suppl. Table 2. Zircon U-Pb analysis of the Mado MM OCC gabbro samples.

Acknowledgements

We are grateful to the officers and crew of the *R/V Hakuho-maru* and *R/V Yokosuka*, and to the operation team of the HOV *Shinkai 6500*, for their professional support in data acquisition. We thank all shipboard scientific members of KH-18-02, YK18-07, YK19-04S, and YK20-18S for collaboration. H. Yamashita, Y. Harigane, and K. Michibayashi kindly provided detailed information on rock samples. The comments from two anonymous reviewers are very helpful. The GMT software (Wessel et al. 2019) was extensively used in this study.

Author contributions

KO and YO proposed the topic and conceived and designed the study. MF conducted field observations. FZ carried out the magnetic forward modeling, and MF collaborated on the interpretation. KT was in charge of age dating and OI helped with the interpretation. TH and YM helped with the onboard geophysical surveys. All authors read and approved the final manuscript.

Funding

This work was supported by JSPS KAKENHI Grant Number 18H010303 "MOW-ALL" and 18K13638.

Availability of data and materials

Bathymetry grid, total magnetic anomaly, reduction to pole anomaly grid, shipboard gravity anomaly, free-air, and Mantle Bouguer anomaly grids are available on PANGAEA, <https://doi.pangaea.de/10.1594/PANGAEA.960003>. Other datasets are available from the corresponding author on reasonable request. All data related to the age dating are included in this published article and its supplementary information files.

Declarations

Competing interests

The authors declare that they have no competing interest.

Author details

¹Atmosphere and Ocean Research Institute, The University of Tokyo, 5-1-5 Kashiwanoha, Kashiwa, Chiba 277-8564, Japan. ²National Museum of Nature

and Science, 4-1-1 Amakubo, Tsukuba, Ibaraki 305-0005, Japan. ³National Institute of Polar Research, 10-3 Midori-cho, Tachikawa, Tokyo 190-8518, Japan. ⁴Graduate University for Advanced Studies (SOKENDAI), 10-3 Midori-cho, Tachikawa, Tokyo 190-8518, Japan. ⁵Institute de Physique du Globe de Paris, 1 rue Jussieu, 75238 Paris Cedex 05, France. ⁶Geological Survey of Japan, National Institute of Advanced Industrial Science and Technology (AIST), Central 7, 1-1-1 Higashi, Tsukuba, Ibaraki 305-0005, Japan. ⁷Hydrographic and Oceanographic Department, 3-1-1 Kasumigaseki, Chiyoda, Tokyo 100-8932, Japan. ⁸Research Institute for Marine Geodynamics, Japan Agency for Marine-Earth Science and Technology, Yokosuka 237-0061, Japan. ⁹Department of Earth and Planetary Sciences, Nagoya University, Nagoya 464-8601, Japan. ¹⁰Kobe Ocean-Bottom Exploration Center, Kobe University, 5-1-1 Fukae-minami-machi, Higashinada-ku, Kobe, Hyogo 658-0022, Japan. ¹¹Graduate School of Science, Tohoku University, 6-3 Aramaki Aza-Aoba, Aoba-ku, Sendai 980-8578, Japan.

Received: 30 March 2023 Accepted: 6 July 2023

Published online: 14 July 2023

References

- Akizawa N, Ohara Y, Okino K, Ishizuka O, Yamashita H, Machida S, Sanfilippo A, Basch V, Snow JE, Sen A, Hirachi K, Michibayashi K, Harigane Y, Fujii M, Asanuma H, Hirata T (2021) Geochemical characteristics of back-arc basin lower crust and upper mantle at final spreading stage of Shikoku Basin: an example of Mado Megamullion. *Prog Earth Planet Sci*. <https://doi.org/10.1186/s40645-021-00454-3>
- Alken P, Thébault E, Beggan CD, Amit A, Aubert J, Baerunzung J, Bondar TN, Brown WJ, Califf F, Chambodut A, Chulliat A, Cox GA, Finlay CC, Fournier A, Gillet N, Grayver A, Hammer MD, Holschneider M, Huder L, Hulot G, Jager T, Kloss C, Langlais B, Leger JM, Lesur V, Livermore PW, Lowes FJ, Macmillan S, Magnes W, Mandea M (2021) International Geomagnetic Reference Field: the thirteenth generation. *Earth Planets Space* 73:49. <https://doi.org/10.1186/s40623-020-01288-x>
- Allerton S, Escartin J, Searle RC (2000) Extremely asymmetric magmatic accretion of oceanic crust at the ends of slow-spreading ridge-segments. *Geology* 28:179–182. <https://doi.org/10.1130/0091-7613>
- Andreani M, Escartin J, Delacour A, Ildefonso B, Godard M, Dymont J, Fallick AE, Fouquet Y (2014) Tectonic structure, lithology, and hydrothermal signature of the Rainbow massif (Mid-Atlantic Ridge 36° 14' N). *Geochem Geophys Geosyst* 15:3543–3571. <https://doi.org/10.1002/2014GC005269>
- Arai R, Dunn RA (2014) Seismological study of Lau back arc crust: Mantle water, magmatic differentiation, and a compositionally zoned basin. *Earth Planet Sci Lett* 390:304–317. <https://doi.org/10.1016/j.epsl.2014.01.014>
- Baines AG, Cheadle MJ, John BE, Schwartz JJ (2008) The rate of oceanic detachment faulting at Atlantis Bank, SW Indian Ridge. *Earth Planet Sci Lett* 273:105–114. <https://doi.org/10.1016/j.epsl.2008.06.013>
- Basch V, Sanfilippo A, Sani C, Ohara Y, Snow J, Ishizuka O, Harigane Y, Michibayashi K, Sen A, Akizawa N, Okino K, Fujii M, Yamashita H (2020) Crustal accretion in a slow-spreading back-arc basin: insights from the Mado Megamullion oceanic core complex in the Shikoku Basin. *Geochem Geophys Geosyst* 21:1–24. <https://doi.org/10.1029/2020gc009199>
- Buck WR (1988) Flexural rotation of normal faults. *Tectonics* 7:959–973
- Buck WR, Lavie LL, Poliakov ANB (2005) Modes of faulting at mid-ocean ridges. *Nature* 434:719–723. <https://doi.org/10.1038/nature03358>
- Cann JR, Blackman DK, Smith DK, McAllister E, Janssen B, Mello S, Avgerinos E, Pascoe AR, Escartin J (1997) Corrugated slip surfaces formed at ridge-transform intersections on the Mid-Atlantic Ridge. *Nature* 385:329–332. <https://doi.org/10.1038/385329a0>
- Cann JR, Smith DK, Escartin J, Schouten H (2015) Tectonic evolution of 200 km of Mid-Atlantic Ridge over 10 million years: interplay of volcanism and faulting. *Geochem Geophys Geosyst* 16:2303–2321. <https://doi.org/10.1002/2015GC005797>. Received
- Cannat M, Mangeny A, Ondréas H, Fouquet Y, Normand A (2013) High-resolution bathymetry reveals contrasting landslide activity shaping the walls of the Mid-Atlantic Ridge axial valley. *Geochem Geophys Geosyst*. <https://doi.org/10.1002/ggge.20056>
- Cannat M, Sauter D, Mendel V, Ruellan E, Okino K, Escartin J, Combier V, Baala M (2006) Modes of seafloor generation at a melt-poor

- ultraslow-spreading ridge. *Geology* 34:605. <https://doi.org/10.1130/G22486.1>
- Chase CG (1978) Extension behind island arcs and motions relative to hot spots. *J Geophys Res* 83:5385. <https://doi.org/10.1029/JB083iB11p05385>
- Collins JA, Blackman DK, Harris A, Carlson RL (2009) Seismic and drilling constraints on velocity structure and reflectivity near IODP Hole U1309D on the central dome of Atlantis Massif, Mid-Atlantic Ridge 30° N. *Geochem Geophys Geosyst.* <https://doi.org/10.1029/2008GC002121>
- Collins JA, Smith DK, McGuire JJ (2012) Seismicity of the Atlantis Massif detachment fault, 30° N at the Mid-Atlantic Ridge. *Geochem Geophys Geosyst.* <https://doi.org/10.1029/2012GC004210>
- Corbalán A, Nedimović MR, Loudon KE, Cannat M, Grevemeyer I, Watremez L, Leroy S (2021) Seismic velocity structure along and across the ultraslow-spreading Southwest Indian Ridge at 64° 30' E showcases flipping detachment faults. *J Geophys Res Solid Earth* 126:1–24. <https://doi.org/10.1029/2021jb022177>
- Craig TJ, Parnell-Turner R (2017) Depth-varying seismogenesis on an oceanic detachment fault at 13° 20' N on the Mid-Atlantic Ridge. *Earth Planet Sci Lett* 479:60–70. <https://doi.org/10.1016/j.epsl.2017.09.020>
- Deschamps A, Fujiwara T (2003) Asymmetric accretion along the slow-spreading Mariana Ridge. *Geochem Geophys Geosyst* 4:1–11. <https://doi.org/10.1029/2003GC000537>
- Deschamps A, Lallemand S (2002) The West Philippine Basin: an Eocene to Early Oligocene back arc basin opened between two opposed subduction zones. *J Geophys Res.* <https://doi.org/10.1029/2001JB001706>
- Deschamps A, Lallemand S, Dominguez S (1999) The last spreading episode of the West Philippine Basin revisited. *Geophys Res Lett* 26:2073–2076
- Deschamps A, Okino K, Fujioka K (2002) Late amagmatic extension along the central and eastern segments of the West Philippine Basin fossil spreading axis. *Earth Planet Sci Lett* 203:277–293. [https://doi.org/10.1016/S0012-821X\(02\)00855-5](https://doi.org/10.1016/S0012-821X(02)00855-5)
- Dick HJB, Tivey MA, Tucholke BE (2008) Plutonic foundation of a slow-spreading ridge segment: oceanic core complex at Kane Megamullion, 23° 30' N, 45° 20' W. *Geochem Geophys Geosyst.* <https://doi.org/10.1029/2007GC001645>
- Dunn RA, Arai R, Eason DE, Canales JP, Sohn RA (2017) Three-dimensional seismic structure of the Mid-Atlantic Ridge: an investigation of tectonic, magmatic, and hydrothermal processes in the Rainbow area. *J Geophys Res Solid Earth.* <https://doi.org/10.1002/2017JB015051>
- Eason DE, Dunn RA, Pablo Canales J, Sohn RA (2016) Segment-scale variations in seafloor volcanic and tectonic processes from multibeam sonar imaging, Mid-Atlantic Ridge Rainbow region (35° 45'–36° 35' N). *Geochem Geophys Geosyst.* <https://doi.org/10.1002/2016GC006433>
- Elsasser WM (1971) Sea-floor spreading as thermal convection. *J Geophys Res* 76:1101–1112. <https://doi.org/10.1029/JB076i005p01101>
- Escartín J, John B, Cannat M, Olive JA, Cheadle M, Fruh-Green G, Cotterill C (2022) Tectonic termination of oceanic detachment faults, with constraints on tectonic uplift and mass wasting related erosion rates. *Earth Planet Sci Lett* 584:117449. <https://doi.org/10.1016/j.epsl.2022.117449>
- Escartín J, Mével C, Petersen S, Bonnemains D, Cannat M, Andreani M, Augustin N, Bezos A, Chavangac V, Choi Y, Godard M, Haaga K, Hamelin C, Ildefonse B, Jamieson B, Leleu T, MacLeod CJ, Massot-Campos M, Nomikou P, Olive JA, Paquet M, Rommevaux C, Rothenbeck M, Steinfuhrer A, Tominaga M, Triebe L, Campos R, Gracias N, Garcia R (2017) Tectonic structure, evolution, and the nature of oceanic core complexes and their detachment fault zones (13° 20' N and 13° 30' N, Mid-Atlantic Ridge). *Geochem Geophys Geosyst* 18:1451–1482. <https://doi.org/10.1002/2016GC006775>
- Escartín J, Smith DK, Cann J, Schouten H, Langmuir CH, Escrig S (2008) Central role of detachment faults in accretion of slow-spreading oceanic lithosphere. *Nature* 455:790–794. <https://doi.org/10.1038/nature07333>
- Fryer P (1996) Evolution of the Mariana convergent plate margin system. *Rev Geophys* 34:89–125
- Fujioka K, Okino K, Kanamatsu T, Ohara Y, Ishizuka O, Haraguchi S, Ishii T (1999) Enigmatic extinct spreading center in the West Philippine backarc basin unveiled. *Geology* 27:1135–1138
- Fujiwara T, Umino S, Asada M et al (2008) A submersible study of the Mariana Trough back-arc spreading center at 17° N. *JAMSTEC Report Res Dev* 8:61–73. <https://doi.org/10.5918/jamstecr.8.61>
- Gong X, Tian L, Dong Y (2022) Contrasting melt percolation and melt-rock reactions in the Parece Vela back-arc oceanic lithosphere, Philippine Sea: a mineralogical perspective. *Lithos* 422–423:106727. <https://doi.org/10.1016/j.lithos.2022.106727>
- Gràcia E, Charlou JL, Radford-Knoery J, Parson LM (2000) Non-transform offsets along the Mid-Atlantic Ridge south of the Azores (38–34°N): ultramafic exposures and hosting of hydrothermal vents. *Earth Planet Sci Lett* 177:89–103. [https://doi.org/10.1016/S0012-821X\(00\)00034-0](https://doi.org/10.1016/S0012-821X(00)00034-0)
- Gracia E, Charlou JL, Radford-Knoery J, Parson LM (2000) Non-transform offsets along the Mid-Atlantic Ridge south of the Azores (38–34°N): ultramafic exposures and hosting of hydrothermal vents. *Earth Planet Sci Lett* 177:89–103
- Grevemeyer I, Hayman NW, Peirce C, Schwardt M, Van Avendonk HJA, Danowski A, Papenberg C (2018) Episodic magmatism and serpentinized mantle exhumation at an ultraslow-spreading centre. *Nat Geosci* 11:444–448. <https://doi.org/10.1038/s41561-018-0124-6>
- Grimes CB, John BE, Cheadle MJ, Wooden JL (2008) Protracted construction of gabbroic crust at a slow spreading ridge: constraints from 206 Pb/238 U zircon ages from Atlantis Massif and IODP Hole U1309D (30°N, MAR). *Geochem Geophys Geosyst.* <https://doi.org/10.1029/2008GC002063>
- Hall CE, Gurnis M, Sdrolias M, Lavier LL, Müller RD (2003) Catastrophic initiation of subduction following forced convergence across fracture zones. *Earth Planet Sci Lett* 212:15–30. [https://doi.org/10.1016/S0012-821X\(03\)00242-5](https://doi.org/10.1016/S0012-821X(03)00242-5)
- Harigane Y, Abe N, Michibayashi K, Kimura J, Chang Q (2016) Melt-rock interactions and fabric development of peridotites from North Pond in the Kane area, Mid-Atlantic Ridge: implications of microstructural and petrological analyses of peridotite samples from IODP Hole U1382A. *Geochem Geophys Geosyst* 17:2298–2322. <https://doi.org/10.1002/2016GC006429>
- Harigane Y, Michibayashi K, Ohara Y (2011a) Relicts of deformed lithospheric mantle within serpentinites and weathered peridotites from the Godzilla Megamullion, Parece Vela Back-arc Basin, Philippine Sea. *Island Arc* 20:174–187. <https://doi.org/10.1111/j.1440-1738.2011.00759.x>
- Harigane Y, Michibayashi K, Ohara Y (2008) Shearing within lower crust during progressive retrogression: Structural analysis of gabbroic rocks from the Godzilla Mullion, an oceanic core complex in the Parece Vela backarc basin. *Tectonophysics* 457:183–196. <https://doi.org/10.1016/j.tecto.2008.06.009>
- Harigane Y, Michibayashi K, Ohara Y (2011b) Deformation and hydrothermal metamorphism of gabbroic rocks within the Godzilla Megamullion, Parece Vela Basin, Philippine Sea. *Lithos* 124:185–199. <https://doi.org/10.1016/j.lithos.2011.02.001>
- Harigane Y, Michibayashi K, Ohara Y (2010) Amphibolitization within the lower crust in the termination area of the Godzilla Megamullion, an oceanic core complex in the Parece Vela Basin. *Island Arc* 19:718–730. <https://doi.org/10.1111/j.1440-1738.2010.00741.x>
- Harigane Y, Okamoto A, Morishita T, Snow JE, Tamura A, Yamashita H, Michibayashi K, Ohara Y, Arai S (2019) Melt–fluid infiltration along detachment shear zones in oceanic core complexes: Insights from amphiboles in gabbro mylonites from the Godzilla Megamullion, Parece Vela Basin, the Philippine Sea. *Lithos* 344–345:217–231. <https://doi.org/10.1016/j.lithos.2019.06.019>
- Haughton GA, Hayman NW, Searle RC, Le Bas T, Murton BJ (2019) Volcanic-tectonic structure of the Mount Dent oceanic core complex in the ultraslow Mid-Cayman Spreading Center determined from detailed seafloor investigation. *Geochem Geophys Geosyst* 20:1298–1318. <https://doi.org/10.1029/2018GC008032>
- Hayman NW, Grindlay NR, Perfit MR, Mann P, Leroy S, Mercier de Lepinay B (2011) Oceanic core complex development at the ultraslow spreading Mid-Cayman Spreading Center. *Geochem Geophys Geosyst* 12:1–21. <https://doi.org/10.1029/2010GC003240>
- Hilde TWC, Lee CS (1984) Origin and evolution of the West Philippine Basin—a new interpretation. *Tectonophysics* 102:85–104. [https://doi.org/10.1016/0040-1951\(84\)90009-X](https://doi.org/10.1016/0040-1951(84)90009-X)
- Hirauchi K, Segawa I, Kouketsu Y, Harigane Y, Ohara Y, Snow J, Sen A, Fujii M, Okino K (2021) Alteration processes recorded by back-arc mantle peridotites from oceanic core complexes Shikoku Basin, Philippine Sea. *Island Arc.* <https://doi.org/10.1111/iar.12419>
- Hochstaedter AG, Gill JB, Taylor B, Ishizuka O, Yuasa M, Morita S (2000) Across-arc geochemical trends in the Izu–Bonin arc: constraints on source

- composition and mantle melting. *J Geophys Res* 105:495–512. <https://doi.org/10.1029/1999JB900125>
- Howell SM, Olive J-A, Ito G, Behn MD, Escartin J, Kaus B (2019) Seafloor expression of oceanic detachment faulting reflects gradients in mid-ocean ridge magma supply. *Earth Planet Sci Lett* 516:176–189. <https://doi.org/10.1016/j.epsl.2019.04.001>
- Isezaki N (1986) A new shipboard three-component magnetometer. *Geophysics* 51:1992–1998. <https://doi.org/10.1190/1.1442054>
- Ishii K, Wallis SR (2022) A possible mechanism for spontaneous cyclic back-arc spreading. *Prog Earth Planet Sci* 9:27. <https://doi.org/10.1186/s40645-022-00486-3>
- Ishii T, Sato H, Machida S et al (2000) Geological and petrological studies of the Kinan and Izu-Ogasawara-back arc–echelon Seamount Chains. *Bull Geol Surv Jpn* 51(12):615–630
- Ishizuka O, Ohara Y, Sato H, Okino K (2004) “Rejuvenated” volcanism in the Parece vela backarc basin: Its timing and chemical characteristics. *Asia Oceania Geophysical Society, first annual meeting 57-OSE-A1500*
- Ishizuka O, Taylor RN, Yuasa M, Ohara Y (2011) Making and breaking an island arc: a new perspective from the Oligocene Kyushu–Palau arc, Philippine Sea. *Geochem Geophys Geosyst* 12:1–40. <https://doi.org/10.1029/2010GC003440>
- Ishizuka O, Uto K, Yuasa M, Hochstaedter AG (1998) Thematic Article K–Ar ages from seamount chains in the back-arc region of the Izu–Ogasawara arc. *Island Arc* 7:408–421
- Ishizuka O, Yuasa M, Taylor RN, Sakamoto I (2009) Two contrasting magmatic types coexist after the cessation of back-arc spreading. *Chem Geol* 266:274–296. <https://doi.org/10.1016/j.chemgeo.2009.06.014>
- Karson JA, Früh-Green GL, Kelley DS, Williams EA, Yoerger DR, Jakuba M (2006) Detachment shear zone of the Atlantis Massif core complex, Mid-Atlantic Ridge, 30° N. *Geochem Geophys Geosyst*. <https://doi.org/10.1029/2005GC001109>
- Kasuga S, Ohara Y (1997) A new model of back-arc spreading in the Parece Vela Basin, northwest Pacific margin. *Island Arc* 6:316–326
- Kitada K, Seama N, Yamazaki T, Nogi Y, Suyehiro K (2006) Distinct regional differences in crustal thickness along the axis of the Mariana Trough, inferred from gravity anomalies. *Geochem Geophys Geosyst* 7:1–14. <https://doi.org/10.1029/2005GC001119>
- Korenaga J (1995) Comprehensive analysis of marine magnetic vector anomalies. *J Geophys Res* 100:365–378
- Kuo BY, Forsyth DW (1988) Gravity-anomalies of the ridge-transform system in the South-Atlantic between 31° S and 34.5° S—Upwelling centers and variations in crustal thickness. *Mar Geophys Res* 10:205–232
- Lallemant S (2016) Philippine Sea Plate inception, evolution, and consumption with special emphasis on the early stages of Izu–Bonin–Mariana subduction. *Prog Earth Planet Sci* 3:15. <https://doi.org/10.1186/s40645-016-0085-6>
- Lissenberg CJ, Rioux M, MacLeod CJ, Bowring SA, Shimizu N (2016) Crystallization depth beneath an oceanic detachment fault (ODP Hole 923A, Mid-Atlantic Ridge). *Geochem Geophys Geosyst* 17:162–180. <https://doi.org/10.1002/2015GC006027>
- Loocke M, Snow JE, Ohara Y (2013) Melt stagnation in peridotites from the Godzillia Megamullion Oceanic Core Complex, Parece Vela Basin, Philippine Sea. *Lithos* 182–183:1–10. <https://doi.org/10.1016/j.lithos.2013.09.005>
- Macdonald KCC, Miller SPP, Huestis SPP, Spiess FNN (1980) Three-dimensional modeling of a magnetic reversal boundary from inversion of deep-tow measurements. *J Geophys Res* 85:3670–3680. <https://doi.org/10.1029/JB085iB07p03670>
- Mallows C, Searle RC (2012) A geophysical study of oceanic core complexes and surrounding terrain, Mid-Atlantic Ridge 13°N–14°N. *Geochem Geophys Geosyst* 13:1–27. <https://doi.org/10.1029/2012GC004075>
- Molnar P, Atwater T (1978) Interarc spreading and Cordilleran tectonics as alternates related to the age of subducted oceanic lithosphere. *Earth Planet Sci Lett* 41:330–340. [https://doi.org/10.1016/0012-821X\(78\)90187-5](https://doi.org/10.1016/0012-821X(78)90187-5)
- Morris A, Gee JS, Pressling N, John BE, MacLeod CJ, Grimes CB, Searle RC (2009) Footwall rotation in an oceanic core complex quantified using reoriented Integrated Ocean Drilling Program core samples. *Earth Planet Sci Lett* 287:217–228. <https://doi.org/10.1016/j.epsl.2009.08.007>
- Mrozowski CL, Hayes DE (1979) The evolution of the Parece Vela Basin, eastern Philippine Sea. *Earth Planet Sci Lett* 46:49–67. [https://doi.org/10.1016/0012-821X\(79\)90065-7](https://doi.org/10.1016/0012-821X(79)90065-7)
- Nakakuki T, Mura E (2013) Dynamics of slab rollback and induced back-arc basin formation. *Earth Planet Sci Lett* 361:287–297. <https://doi.org/10.1016/j.epsl.2012.10.031>
- Nooner SL, Sasagawa GS, Blackman DK, Zumberge MA (2003) Structure of oceanic core complexes: Constraints from seafloor gravity measurements made at the Atlantis Massif. *Geophys Res Lett* 30:8–11. <https://doi.org/10.1029/2003GL017126>
- Ohara Y (2016) The Godzillia Megamullion, the largest oceanic core complex on the earth: a historical review. *Island Arc* 25:193–208. <https://doi.org/10.1111/iar.12116>
- Ohara Y (2021) IODP drilling at the godzilla megamullion: the nature of the backarc basin lower crust and upper mantle. *J Geogr (Chigaku Zasshi)* 130(4):543–558. <https://doi.org/10.5026/jgeography.130.543>
- Ohara Y, Fujioka K, Ishii T, Yurimoto H (2003) Peridotites and gabbros from the Parece Vela backarc basin: Unique tectonic window in an extinct backarc spreading ridge. *Geochem Geophys Geosyst*. <https://doi.org/10.1029/2002GC000469>
- Ohara Y, Kato Y, Yoshida T, Nishimura A (2015) Geoscientific characteristics of the seafloor of the Southern Ocean of Japan revealed by Japan’s continental shelf survey. *J Geogr (Chigaku Zasshi)* 124:687–709. <https://doi.org/10.5026/jgeography.124.687>
- Ohara Y, Okino K, Snow JE (2011) Tectonics of unusual crustal accretion in the Parece Vela Basin. In: Ogawa Y, Anma R, Dilek Y (eds) *Accretionary prisms and convergent margin tectonics in the Northwest Pacific Basin*. Springer, Dordrecht, pp 149–168
- Ohara Y, Yoshida T, Kato Y, Kasuga S (2001) Giant megamullion in the Parece Vela backarc basin. *Mar Geophys Res* 22:47–61. <https://doi.org/10.1023/A:1004818225642>
- Okino K (2015) Magnetic anomalies in the Philippine Sea: implications for regional tectonics. *J Geogr (Chigaku Zasshi)* 124:729–747. <https://doi.org/10.5026/jgeography.124.729>
- Okino K, Fujioka K (2003) The Central Basin Spreading Center in the Philippine Sea: structure of an extinct spreading center and implications for marginal basin formation. *J Geophys Res* 108:1–18. <https://doi.org/10.1029/2001JB001095>
- Okino K, Kasuga S, Ohara Y (1998) A new scenario of the Parece Vela Basin genesis. *Mar Geophys Res* 20:21–40. <https://doi.org/10.1023/A:1004377422118>
- Okino K, Matsuda K, Christie DM, Nogi Y, Koizumi K (2004) Development of oceanic detachment and asymmetric spreading at the Australian–Antarctic Discordance. *Geochem Geophys Geosyst*. <https://doi.org/10.1029/2004GC000793>
- Okino K, Ohara Y, Kasuga S, Kato Y (1999) The Philippine Sea: new survey results reveal the structure and the history of the marginal basins. *Geophys Res Lett* 26:2287–2290. <https://doi.org/10.1029/1999GL900537>
- Okino K, Shimakawa Y, Nagaoka S, Shinji N (1994) Evolution of the Shikoku Basin. *J Geomagn Geoelectr* 46:463–479. <https://doi.org/10.1017/CBO9781107415324.004>
- Parker RL, Huestis SP (1974) The inversion of magnetic-anomalies in presence of topography. *J Geophys Res* 79:1587–1593
- Parnell-Turner R, Sohn RA, Peirce C, Reston TJ, MacLeod CJ, Searle RC, Simao NM (2017) Oceanic detachment faults generate compression in extension. *Geology* 45:923–926. <https://doi.org/10.1130/G39232.1>
- Paulatto M, Canales JP, Dunn RA, Sohn RA (2015) Heterogeneous and asymmetric crustal accretion: New constraints from multibeam bathymetry and potential field data from the Rainbow area of the Mid-Atlantic Ridge (36°15′N). *Geochem Geophys Geosyst* 16:2994–3014. <https://doi.org/10.1002/2015GC005743>
- Pressling N, Morris A, John BE, MacLeod CJ (2012) The internal structure of an oceanic core complex: an integrated analysis of oriented borehole imagery from IODP Hole U1309D (Atlantis Massif). *Geochem Geophys Geosyst* 13:Q04G10. <https://doi.org/10.1029/2012GC004061>
- Ranero CR, Reston TJ (1999) Detachment faulting at ocean core complexes. *Geology* 27:983–986
- Sasaki T, Yamazaki T, Ishizuka O (2014) A revised spreading model of the West Philippine Basin. *Earth Planets Space* 66:83. <https://doi.org/10.1186/1880-5981-66-83>

- Sato H, Machida S, Kanayama S, Taniguchi H, Ishii T (2002) Geochemical and isotopic characteristics of the Kinan Seamount Chain in the Shikoku Basin. *Geochem J* 36:519–526. <https://doi.org/10.2343/geochemj.36.519>
- Sato T, Okino K, Kumagai H (2009) Magnetic structure of an oceanic core complex at the southernmost Central Indian Ridge: analysis of ship-board and deep-sea three-component magnetometer data. *Geochem Geophys Geosyst*. <https://doi.org/10.1029/2008GC002267>
- Sauter D, Cannat M, Rouméjon S, Andreani M, Birot D, Bronner A, Brunelli A, Carlut J, Delacour A, Guyader V, MacLeod CJ, Manatschal G, Mendel V, Menez B, Pasini V, Ruellan E, Searle R (2013) Continuous exhumation of mantle-derived rocks at the Southwest Indian Ridge for 11 million years. *Nat Geosci* 6:314–320. <https://doi.org/10.1038/ngeo1771>
- Schellart WP (2005) Influence of the subducting plate velocity on the geometry of the slab and migration of the subduction hinge. *Earth Planet Sci Lett* 231:197–219. <https://doi.org/10.1016/j.epsl.2004.12.019>
- Schellart WP, Moresi L (2013) A new driving mechanism for backarc extension and backarc shortening through slab sinking induced toroidal and poloidal mantle flow: results from dynamic subduction models with an overriding plate. *J Geophys Res Solid Earth* 118:3221–3248. <https://doi.org/10.1002/jgrb.50173>
- Scholz CH, Campos J (1995) On the mechanism of seismic decoupling and back arc spreading at subduction zones. *J Geophys Res* 100:22103–22116. <https://doi.org/10.1029/95JB01869>
- Schroeder T, John BE (2004) Strain localization on an oceanic detachment fault system, Atlantis Massif, 30°N, Mid-Atlantic Ridge. *Geochem Geophys Geosyst*. <https://doi.org/10.1029/2004GC000728>
- Sdrolias M, Müller RD (2006) Controls on back-arc basin formation. *Geochem Geophys Geosyst* 7:2005GC001090. <https://doi.org/10.1029/2005GC001090>
- Sdrolias M, Roest WR, Müller RD (2004) An expression of Philippine Sea plate rotation: the Parece Vela and Shikoku Basins. *Tectonophysics* 394:69–86. <https://doi.org/10.1016/j.tecto.2004.07.061>
- Seama N, Nogi Y, Isezaki N (1993) A new method for precise determination of the position and strike of magnetic boundaries using vector data of the geomagnetic anomaly field. *Geophys J Int* 113:155–164
- Searle RC, Bralee AV (2007) Asymmetric generation of oceanic crust at the ultra-slow spreading Southwest Indian Ridge, 64°E. *Geochem Geophys Geosyst* 8:Q05015. <https://doi.org/10.1029/2006GC001529>
- Searle RC, Cannat M, Fujioka K, Mevel C, Fujimoto H, Bralee A, Parson L (2003) FUJI Dome: a large detachment fault near 64°E on the very slow-spreading southwest Indian Ridge. *Geochem Geophys Geosyst*. <https://doi.org/10.1029/2003GC000519>
- Searle RC, MacLeod CJ, Peirce C, Reston TJ (2019) The Mid-Atlantic Ridge near 13° 20' N: High-resolution magnetic and bathymetry Imaging. *Geochem Geophys Geosyst*. <https://doi.org/10.1029/2018GC007940>
- Sen A, Snow JE, Ohara Y, Hirauchi K, Kouketsu Y, Sanfillipino A, Basch V, Harigane M, Fujii M, Okino K, Akizawa N (2021) Melting and evolution of amphibole-rich back-Arc abyssal peridotites at the Mado Megamullion, Shikoku Basin. *Geochem Geophys Geosyst* 22:1–20. <https://doi.org/10.1029/2021gc010013>
- Smith DK, Cann JR, Escartín J (2006) Widespread active detachment faulting and core complex formation near 13 degrees N on the Mid-Atlantic Ridge. *Nature* 442:440–443. <https://doi.org/10.1038/nature04950>
- Smith DK, Schouten H, Dick HJB, Cann JR, Salters V, Marschall HR, Ji F, Yoerger D, Sanfillipino A, Parnell-Turner R, Palmiotto C, Zheleznov A, Bai H, Junkin W, Urann B, Dick S, Sulanowska M, Lemmond P, Curry S (2014) Development and evolution of detachment faulting along 50 km of the Mid-Atlantic Ridge near 16.5° N. *Geochem Geophys Geosyst* 15:4692–4711. <https://doi.org/10.1002/2014GC005563>
- Spencer JE, Ohara Y (2014) Curved grooves at the Godzilla Megamullion in the Philippine Sea and their tectonic significance. *Tectonics* 33:1028–1038. <https://doi.org/10.1002/2013TC003515>
- Takahashi N, Kodaira S, Tatsumi Y, Yamashita M, Sato T, Kaiho Y, Miura S, No T, Takizawa K, Kaneda Y (2009) Structural variations of arc crusts and rifted margins in the southern Izu–Ogasawara arc–back arc system. *Geochem Geophys Geosyst*. <https://doi.org/10.1029/2008GC002146>
- Takahashi N, Kodaira S, Tatsumi Y, Kaneda Y, Suyehiro K (2008) Structure and growth of the Izu–Bonin–Mariana arc crust: 1. Seismic constraint on crust and mantle structure of the Mariana arc–back-arc system. *J Geophys Res* 113:1–18. <https://doi.org/10.1029/2007JB005120>
- Tani K, Dunkley DJ, Ohara Y (2011) Termination of backarc spreading: zircon dating of a giant oceanic core complex. *Geology* 39:47–50. <https://doi.org/10.1130/G31322.1>
- Taylor B (1992) Rifting and the volcanic-tectonic evolution of the Izu–Bonin–Mariana Arc. In: Taylor B, Fujioka K et al (eds) Proceedings of the ocean drilling program, scientific results, vol 126. Ocean Drilling Program, College Station, pp 627–651
- Tomoda Y, Kobayashi K, Segawa J, Nomura K, Kimura T, Saki T (1975) Linear magnetic-anomalies in Shikoku Basin, northeastern Philippine Sea. *J Geomagn Geoelectr* 27:47–56. <https://doi.org/10.5636/jgg.27.47>
- Tucholke BE, Behn MD, Buck WR, Lin J (2008) Role of melt supply in oceanic detachment faulting and formation of megamullions. *Geology* 36:455. <https://doi.org/10.1130/G24639A.1>
- Tucholke BE, Lin J, Kleinrock MC (1998) Megamullions and mullion structure defining oceanic metamorphic core complexes on the Mid-Atlantic Ridge. *J Geophys Res Solid Earth* 103:9857–9866. <https://doi.org/10.1029/98JB00167>
- Wessel P, Luis JF, Uieda L, Scharroo R, Wobbe F, Smith WHF, Tian D (2019) The generic mapping tools version 6. *Geochem Geophys Geosyst* 20:5556–5564. <https://doi.org/10.1029/2019GC008515>
- Xu M, Tivey MA (2016) Investigation of a marine magnetic polarity reversal boundary in cross section at the northern boundary of the Kane Megamullion, Mid-Atlantic Ridge, 23°40'N. *J Geophys Res Solid Earth* 121:3161–3176. <https://doi.org/10.1002/2016JB012928>
- Xu M, Zhao X, Canales JP (2020) Structural variability within the Kane oceanic core complex from full waveform inversion and reverse time migration of streamer data. *Geophys Res Lett*. <https://doi.org/10.1029/2020GL087405>
- Yamazaki T, Chiyonobu S, Ishizuka O, Tajima F, Uto N, Takagawa S (2021) Rotation of the Philippine Sea plate inferred from paleomagnetism of oriented cores taken with an ROV-based coring apparatus. *Earth Planets Space*. <https://doi.org/10.1186/s40623-021-01490-5>
- Yamazaki T, Murakami F (1998) Asymmetric rifting of the northern Mariana Trough. *Island Arc* 7:460–470
- Zhou F, Dymant J (2022) Variability of sea-surface magnetic anomalies at ultraslow spreading centers: consequence of detachment faulting and contrasted magmatism? *Geophys Res Lett*. <https://doi.org/10.1029/2021gl097276>
- Zhou F, Dymant J, Tao C, Wu T (2022) Magmatism at oceanic core complexes on the ultraslow Southwest Indian Ridge: insights from near-seafloor magnetism. *Geology* 50:726–736. <https://doi.org/10.1130/G49771.1>

Publisher's Note

Springer Nature remains neutral with regard to jurisdictional claims in published maps and institutional affiliations.

Submit your manuscript to a SpringerOpen® journal and benefit from:

- Convenient online submission
- Rigorous peer review
- Open access: articles freely available online
- High visibility within the field
- Retaining the copyright to your article

Submit your next manuscript at ► [springeropen.com](https://www.springeropen.com)